Supporting Information

Rescaling of metal oxide nanocrystals for energy storage having high capacitance and energy density with robust cycle life

Hyung Mo Jeong[a], Kyung Min Choi[a], Tao Cheng[b], Dong Ki Lee[a], Renjia Zhou[c], Il Woo Ock[d], Delia J. Milliron[c,e], William A Goddard III[b,1] and Jeung Ku Kang[a,d,1]

[a] Department of Materials Science and Engineering, Korea Advanced Institute of Science and Technology, Daejeon 305-701, Republic of Korea

[b] Materials and Process Simulation Center, California Institute of Technology, Pasadena, CA 91125

[c] Molecular Foundry, Lawrence Berkeley National Laboratory, Berkeley, CA 94720

[d] Graduate School of Energy, Environment, Water and Sustainability, Korea Advanced Institute of Science and Technology, Daejeon 305-701, Republic of Korea

[e] Department of Chemical Engineering, University of Texas at Austin, Austin, TX 78712

[1] To whom correspondence may be addressed. E-mail: wag@wag.caltech.edu or jeung@kaist.ac.kr

SI Text

S1: Materials and Methods

Synthesis of Nickel Oxide Nanocrystals on Graphene. Graphene oxide was dispersed in water by 1 h of sonication (2, 1, and 0.4 mg ml^{-1} for NiO_{30}-g, NiO_{50}-g, and NiO_{70}-g, 30 ml). Then, appropriate amounts of nickel acetate [$Ni(CH_3COO)_2$ $4H_2O$] (50.9 ml, 10 mM aqueous solution) were added to obtain NiO nanoparticles on the graphene oxide solution. After an additional 30 min of sonication, the mixed solution was reduced with 28 wt. % of ammonium hydroxide solution (2.8 ml) and 35 wt. % of hydrazine solution (15 ml) while stirring for 3 h at 60 °C. Black powders were obtained by filtration, washed with water several times, and dried overnight in a vacuum oven at 60 °C. These steps produced NiO precursors coated on graphene, which were subsequently reduced by thermal chemical vapor deposition (CVD) under a hydrogen atmosphere at 300 °C for 3 h. The final products were obtained after an additional heat treatment of approximately 2 h under air at 250 °C. The mass of NiO particles on graphene was obtained by thermogravimetric analysis.

X-Ray Diffraction Measurement. Powder X-ray data were collected using a SmartLab θ-2θ diffractometer in the reflectance Bragg-Brentano geometry employing a Johansson type Ge (111) monochromator filtered Cu Kα1 radiation at 1200W (40 kV, 30 mA) power and equipped with a high speed 1D detector (D/teX Ultra). The desquamated powder from the NiO on graphene was held in a holder stage and scanned by the scan speed of 2 °min in a continuous mode (Fig. S2).

Cs-TEM (Transmission Electron Microscopy). For the TEM observation (JEM-ARM200F produced by JEOL), NiO on graphene was divided into small pieces after being stripped away from the substrate and then dispersed with the acetone solvent on a TEM mesh grid.

XPS (X-ray Photoelectron Spectroscopy). XPS spectra were obtained using a Sigma Probe from Thermo VG Scientific, which is equipped with a 350 W Al anode X-ray source along with a multi-anode, a pulse counting, and a hemispherical analyzer. The spectra were collected using an incident photon energy of 1486.6 eV and were corrected for the detector's work function.

TGA (Thermogravimetric Analysis). The weight fraction of nickel oxide in NiO-n/gr and NiO-a/gr samples were determined by using a TGA (Netzsch, TG 209 F3).

Raman Spectroscopy. The defect or distortion of the graphene in the electrode is observed by Raman spectra. Raman spectra were obtained using a high resolution dispersive Raman microscope (ARAMIS, HORIBA), which is equipped by an Ar ion CW Laser (514.5 nm).

Fourier Transform Infrared Spectroscopy (FTIR). The functional groups present in samples are analyzed by using a FTIR spectroscopy (FT/IR-6100, JASCO).

Surface Area and Pore Size Analyzer. The N_2 adsorption and desorption isotherms were determined using a Quadrasorp SI (Quantachrome Instruments).

Inductively Coupled Plasma (ICP) Optical Emission Spectrometer. For corroborating the contents of the NiO in a sample, the ICP measurements were carried out. The mass concentrations of Ni were measured by the iCAP 6300 Duo (Thermo Scientific).

S2: Experimental Characterization of NiO on Graphene

TEM and PXRD were used to characterize NiO on graphene. Figs. S1 and S2 show TEM images for the size and the shape and PXRD patterns for the crystallinity, respectively.

S3: Electrochemical Fabrication

Lithium Conversion Reaction: The reactions were processed by both cyclic voltammetry and also galvanostatic charge/discharge using a Bio-logic VSP potentiostat with the software by EC-lab Bio-logic, which was connected to a coin cell holder. In cyclic voltammetry measurements, the voltage window is 0.001 to 3.0 V vs. Li/Li^+ at a scan rate of 0.1 mV s^{-1}. Also, galvanostatic measurements were carried out at 0.1 A s^{-1} (~ C/10).

S4: Ex Situ TEM and STEM Analyses

We performed the ex situ TEM analysis to determine structural changes of NiO nanoparticles during lithiation-induced recalling. A 3-nm NiO on graphene sample was prepared on a TEM grid composed of a Cu mesh and a carbon support layer and characterized using Cs-TEM and STEM. Also, the initial structure of a specific NiO particle is imaged using both Cs-TEM and STEM methods and its location is marked to trace the structural change after lithiation. The marked grid was assembled into a coin type cell (CR-2032) with a Li metal foil as a counter electrode, a separator, and the electrolyte. Then, the prepared coin cell was set for the potentiostat measurement and also measured using the cyclic voltammetry at a scan rate of 0.1 mV s^{-1} scan rate (Fig. S4). Next, after electrochemical measurements, the cell was disassembled and the TEM grid was washed with acetone and water to remove the residual electrolyte and Li ions. After washing the grid with water, the grid was used for Cs-TEM analysis and the marked sample was analyzed.

S5: Characterization of NiO-a/gr Samples

The PXRD, XPS, FT-IR, Raman spectra, and BET measurements were performed to analyze the NiO structure, the chemical bonding of NiO on NiO-a/gr, the interaction between NiO and graphene, the defects and distortion of the graphene, and surface properties of a rescaled sample. Meanwhile, PXRD has limitation to resolve atomic ordering in particles below 3-nm. In that reason, we prepared 10-nm sized NiO samples for further clarification by PXRD whether the particles could be created by rescaling. Fig. S9 shows that the 10-nm particles are rescaled into 2 to 3-nm particles after reaction.

S6: Rescaling of Cobalt Oxide Nanoparticles

Synthesis of Cobalt Oxide Particles on Graphene. Graphene oxide was dispersed in water by 1 h of sonication (1 mg ml^{-1}, 30 ml). Then, cobalt acetate [$Co(CH_3COO)_2$ $4H_2$] (51 ml, 10 mM aqueous solution) was added to obtain Co_3O_4 particles in the graphene oxide solution. After an additional 30 min of sonication, the mixed solution was reduced with 28 wt. % ammonium hydroxide solution (2.8 ml) and 35 wt.% hydrazine solution (15 ml) while stirring for 3 h at 60 °C. Black powders were obtained by filtration, washed with water several times, and dried overnight in a vacuum oven at 60 °C. These steps resulted in graphene substrate coated by Co precursors, which was subsequently reduced by thermal chemical vapor deposition (CVD) under a hydrogen atmosphere at 300 °C for 3 h. The final product was obtained after an additional heat treatment of approximately 2 h in air at 250 °C.

S7: Reactive Molecular Dynamic Simulations of Lithium-Induced Rescaling

For these reactive molecular dynamics (RMD) simulations, we have used the reactive force field (ReaxFF) that was trained to reproduce the energetics and barriers from quantum mechanics, The ReaxFF parameters used here is based on a combination of the Ni-C-H-O force field (1) and the Li-C-H-O force field (2), and then further trained to reproduce the bonding energy in OLi_2 and OLi_3^+ finite molecules. The necessary parameters are collected in Table S1 using the format for LAMMPS.

S8: Experimental Conditions for Spectroscopy

Experiments for in situ and ex situ spectroscopy measurements, such as SEC and XPS, are conducted by loading the samples on a gold thin film coated glass substrate. A 1-nm thick Cr thin film was first coated by thermal evaporation (LBNL, Molecular foundry), then the Au was deposited. The Au-coated thin film substrate is very suitable for spectroscopy during lithium charge/discharge because there is no significant reaction between gold and lithium (Fig. S20).

S9: Ex Situ XPS Measurement

Ex situ XPS measurements were conducted at various electrochemical points including the end points of lithiation and delithiation and these data support the progression of the Ni oxidation state from +2 to 0 and 0 to +2 by a reversible conversion reaction, respectively. After lithiation of the samples on the Au-coated glass, the sample was disassembled in the Ar-filled glove and washed by dimethyl carbonate and acetonitrile. Then, the sample was transferred in a glass jar, which was completely sealed in a glove box to prevent contamination. The lithiated sample with the Au glass substrate is put on the XPS holder and connected to the holder via a screw in order to minimize charging effects. After measuring the lithiated sample, the sample was reassembled and was processed by the delithiation (recharging to 3 V vs. Li/Li^+) to finish lithiation-induced rescaling. The measurement of the delithiated sample is conducted by the same process used for the measurements of the lithiated sample. The sample was maintained in an air-free environment aside from the exposure of less than 30 seconds to air for the sample transfer and its loading. Also, the XPS spectra were obtained using a Sigma Probe (Thermo VG Scientific) equipped with a 350 W Al anode x-ray source along with a multi-anode, a pulse counting, and a hemispherical analyzer. Before incident of a probe beam, the Ar ion sputtering has been conducted for 10 sec under 1 keV to remove the SEI layer and any contamination that could result from a side reaction. The spectra were collected using an incident photon energy of 1486.6 eV and were corrected for the detector's work function. In addition, all the spectra were corrected to account for charging by shifting their binding energy such that the center of the C 1s peak lies at 284.5 eV.

S10: Spectroelectrochemistry (SEC) by In Situ & Ex Situ Ultraviolet–Visible (UV/VIS) Transmission Spectroscopy of NiO on Graphene

In Situ Spectroelectrochemistry (SEC). The transparency of NiO on graphene on the Au thin film substrates allows a precise monitoring of the Ni oxidation state. For coupled electrochemical and spectroscopic experiments, the samples were placed in an open quartz cuvette and immersed in a 1M solution of $LiPF_6$ in EC/DEC (1:1 in weight). Li metal foils were used as reference and counter electrodes. The sample acting as the working electrode was subjected to cyclic voltammetry measurement at a scan rate of 1 mV s^{-1} over a voltage range of 0.1 V to 3 V. In situ optical spectra, whose backgrounds are corrected for the Au-coated glass, were collected at particular voltage points during charge and discharge of the sample. The path-length of light through the electrolyte for all measurements was about 1 mm. All the spectra were collected using an ASD Quality Spec Pro UV-Vis-NIR spectrometer.

Ex Situ Spectroelectrochemistry (SEC). For a more accurate measurement of a UV region including the information of the NiO band gap, we have also used the UV spectroscopy (see Fig. S21) at the initial state, the middle of lithiation, the end of lithiation, the middle of delithiation, and the fully delithiation point by the ex situ SEC. The sample was transferred to the UV spectroscopy equipment using the same process as in the case of ex situ XPS.

S11: Graphene Substrate

Synthesis of Graphene Oxide. Graphite was oxidized to graphene oxide by Hummers's method (3). Specifically, 2.0 g of graphite was dipped in an acid solution where $NaNO_3$ (1 g, 11.7 mmol) and $KMnO_4$ (6.3 g, 39.8 mmol) were dissolved in 92 ml of sulfuric acid. The color of the solution turned to yellow-brown. A brown powder was obtained after filtration and washing with water.

S12: Measurement of Surface Faradaic Reactions

To determine the performance of the metal oxide nanoparticles undergoing surface faradaic reactions with OH^- ions, a KOH aqueous electrolyte in a three-electrode supercapacitive system was adopted. A platinum coil, a silver/silver chloride electrode in a saturated KCl solution, and a saturated calomel electrode are used as counter, reference 1, and reference 2 electrodes, respectively. The measurement kit exposed the sample to 1 M KOH aqueous solution electrolyte and the sample plate is sandwiched between the two Teflon cell blocks. The area and the intensity of the cyclic voltammetry (CV) peaks show the activity and the capacity of NiO particles in the surface redox reaction of $NiO + OH^- \rightleftarrows NiOOH + e^-$.

Cyclic Voltammetry Measurement. The capacitive behavior of electrode materials are generally characterized using cyclicvoltammetry (CV). For an electrical double-layer capacitor, the shape of a CV curve is rectangular. In contrast, for a surface Faradaic reaction, large redox peaks exist. The specific capacitance can be calculated from the area under the CV curve using the following equation:

$$C = \frac{1}{2mv(Vf - Vi)} \int_{V_i}^{V_f} I \, dV$$

where m is the mass of the electroactive material in the electrode (g), v is the scan rate (V s^{-1}), V_i is the initial potential (V), V_f is the final potential of CV curve (V), and I is the response current density (A).

Galvanostatic Measurement. The capacitance, the rate capability, and the cycle life were all characterized by galvanostatic measurements (equipment: Bio-logic VSP, software: EC-lab Bio-logic). Various current densities were applied to cells while the potential was swept between cut-off values (0 V ≤ V ≤ 0.5 V). Voltages were recorded at every 0.001 to 0.1 seconds.

Analysis of the Capacitance. The capacitance of each device was calculated from the galvanostatic charge/discharge profile at different currents based on the following equation:

$$C = I / m(-dV/dt)$$

where I is the applied current (A), m is mass of electroactive material in electrode (g), and dV/dt is the slope of the discharged curve (V/s). In addition, the mass of electroactive material has been obtained from the weight fraction of active material in the composite of rescaled particles and the graphene support. It should be noted that the total mass of a NiO_{30}-a/gr, NiO_{50}-a/gr, or NiO_{70}-a/gr electrode was in the range of 1.3 – 1.5 mg per cm^2.

S13: Asymmetric Supercapacitor Full-Cell

Design of an Asymmetric Supercapacitor Full-Cell (NiO-a/gr||NG). To evaluate the possibility of using NiO-a/gr as the electrode in a practical capacitor device, the electrode is integrated in to a coin-type cell. Unlike electrical double layer capacitors or some examples of pseudo-capacitor based on electrodes such as graphene, activated carbon, and MnO_2, it is difficult to design a symmetric two electrode supercapacitor based on NiO electrodes. This is because the redox reaction of NiO cannot accommodate cations from the aqueous electrolyte during charging. Only a small, double layer capacitance would contribute to capacitance at the negative electrode during charging. For this reason, to evaluate the capacitive performance of the NiO-a/gr electrode in a practical device, we fabricated an asymmetric capacitor using NiO-a/gr as the positive electrode and nitrogen-doped graphene (NG) as the negative electrode. The NG electrode when acting as the negative electrode accepts cations from the electrolyte when the cell is charged. Based on the specific capacitance based on CV measurement of each electrode at 5 mV s^{-1} and the principle of charge balance between two electrodes, the mass ratio of NiO_{70}-a/gr to the NG was determined to be 0.286. The total mass of active material on the negative electrode was 2.4 mg cm^{-2} while on the positive electrode it was 0.7 mg cm^{-2}.

Considering the high applied voltage (1.6 V) and whole capacitance, we find that the assembled cell based on NG and NiO_{70}-a/gr gives high performance at both the specific energy density of 78.6 Wh kg^{-1} at an average power density of 951.6 W kg^{-1} and the specific energy density of 33.2 Wh kg^{-1} at an average power density of 21.4 kW kg^{-1}. These specific energy density values obtained using NiO-a/gr as the asymmetric electrodes are very promising. These results support that NiO-a/gr can be adopted as the counter electrode enabling high energy density based on the availability of other high capacitance working electrodes while maintaining high power and long cycle life, thus providing great promise for energy storage devices.

Design of an Asymmetric Supercapacitor Full-Cell (NiO-a/gr||AC). We also fabricated an asymmetric capacitor using NiO-a/gr as the positive electrode and activated carbon (AC) as the negative electrode. Based on the specific capacitance of each electrode and the principle of charge balance between two electrodes, the mass ratio of NiO_{70}-a/gr to the AC was determined to be 0.125 (based on specific capacitance from CV measurement at 5 mV s^{-1}). The total mass of active material on the negative electrode was 5.6 mg cm^{-2} while on the positive electrode it was 0.7 mg cm^{-2}.

Analysis of the Galvanostatic Data. The IR drop at the upper cut-off potential and slope in the discharge curve are used to obtain the average power and energy density. The specific capacitance (Cs) is calculated by using the following equation of

$$Cs = I \times \Delta t / (\Delta V \times M)$$

where I is the current applied, the slope is that of the discharge curve after the IR drop, and M is the total mass of electrode materials. Similarly, the energy density of E is calculated using

$$E = 0.5 C V^2 / M$$

in which V is the cut-off potential excluding the IR drop, M is the total mass of material on both electrode, and C is the measured capacitance. In addition the average power density is calculated by using

$$P = E / \Delta t$$

in which E is the energy density, and Δt is the discharge time after IR drop.

S14: Theoretical and Measured Capacitances

According to the faradaic reaction of NiO + OH^- ⇄ NiOOH + e^- in the KOH aqueous electrolyte, the theoretically available maximum value of a NiO supercapacitive capacitance via an atom-to-atom Faradaic surface reactions is 2,618 F per one gram of NiO under the bias of 0.5 V, based on the following equation of

[Avogadro constant (6.023×10^{23} per mol)] × [1 NiO per mol] × [1 electron per NiO] × [1.623×10^{-19} C per electron] / [74.69 g per 1 mol of NiO] / [0.5 V] = 2,618 F per one gram of NiO, which could be denoted by 2,618 F $g_{NiO70\text{-}a}$. This theoretical capacitance is comparable to the measured capacitance of 3,023 F g^{-1} (the potential window of 0 to 0.5 V) for NiO_{70}-a/gr. Consequently, the measured capacitance shows that lithiation-induced rescaled particles could store the ultimate amount of electrons produced by facilitating entire constituents in particles.

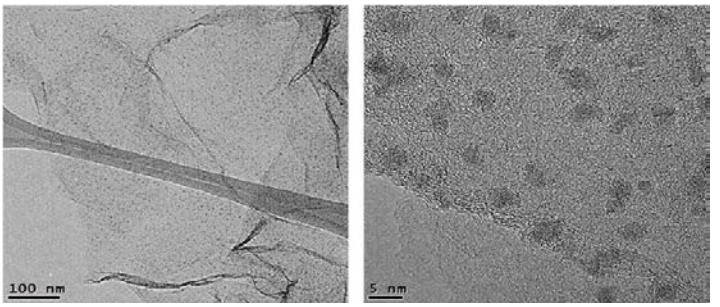

Fig.S1. The size and the shape of NiO on graphene.

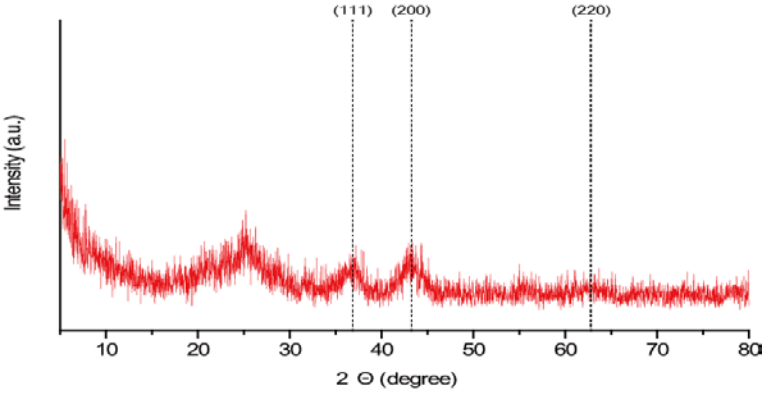

Fig. S2. The PXRD of NiO on graphene. The peak at ~25° is due to the lattice spacing of graphitic carbon, while the labeled peaks correspond to NiO (JCPDS number 71-1179).

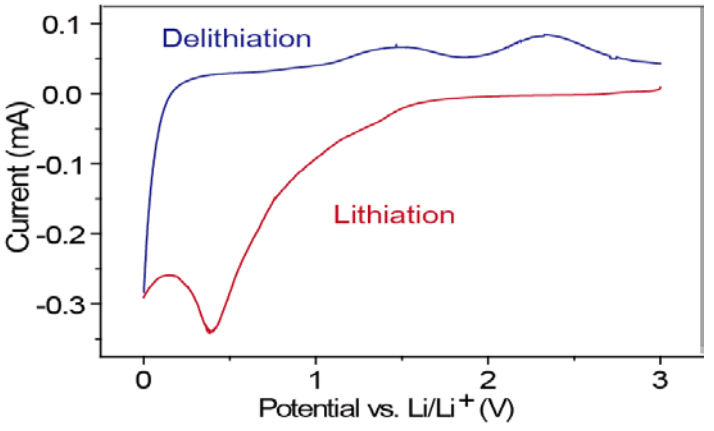

Fig. S3. The voltage profile of NiO on graphene at the first cycle under lithiation rescaling. The plateaus located at around 0.5 V for the discharge curve and at around 1.3 V and 2.3 V for the charge curve of the voltammetry measurements correspond with cathodic and anodic peaks.

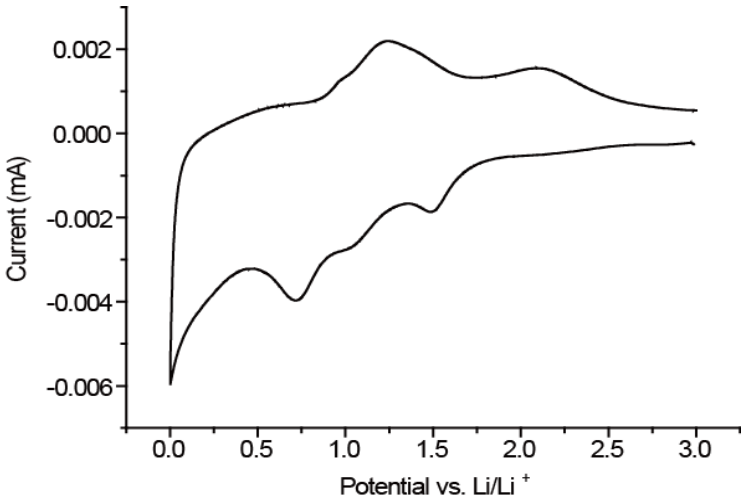

Fig. S4. CV of a 3-nm NiO on graphene sample on a TEM grid. The cathodic and anodic peaks are slightly shifted by the contact resistance between a sample and the grid.

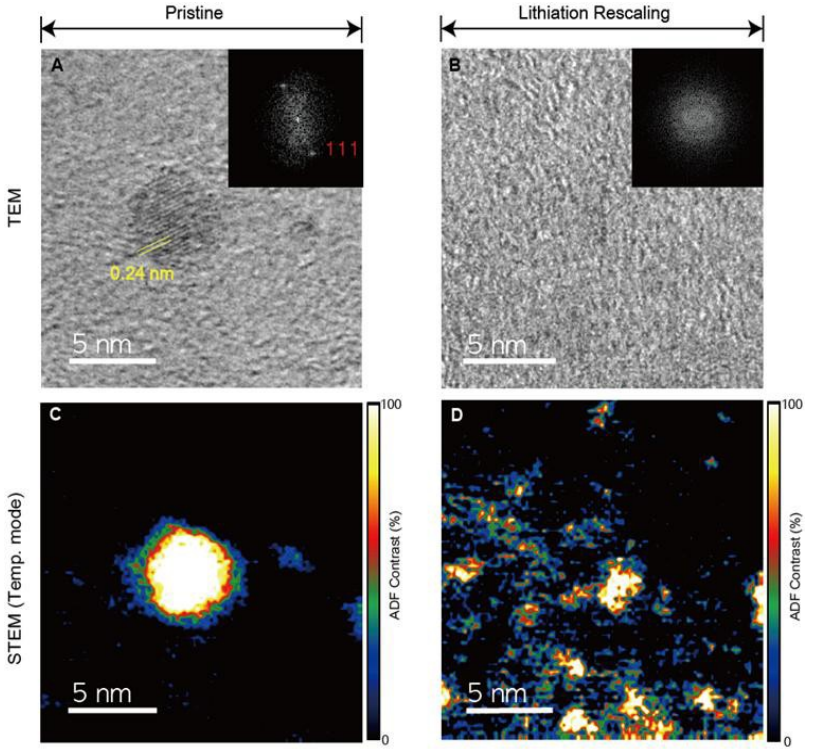

Fig. S5. TEM & STEM characterization of an individual NiO particle at the same spot before and after lithiation-induced rescaling. (*A* and *B*) TEM images of NiO particles (*A*) before and (*B*) after lithiation-induced rescaling. The yellow marks indicate the crystal lattice spacing of a NiO particle. The top right inset shows the FFT diffraction pattern obtained from a single NiO particle. (*C* and *D*) STEM mapping images of NiO particles (*C*) before and (*D*) after lithiation-induced rescaling at the same position for the TEM image.

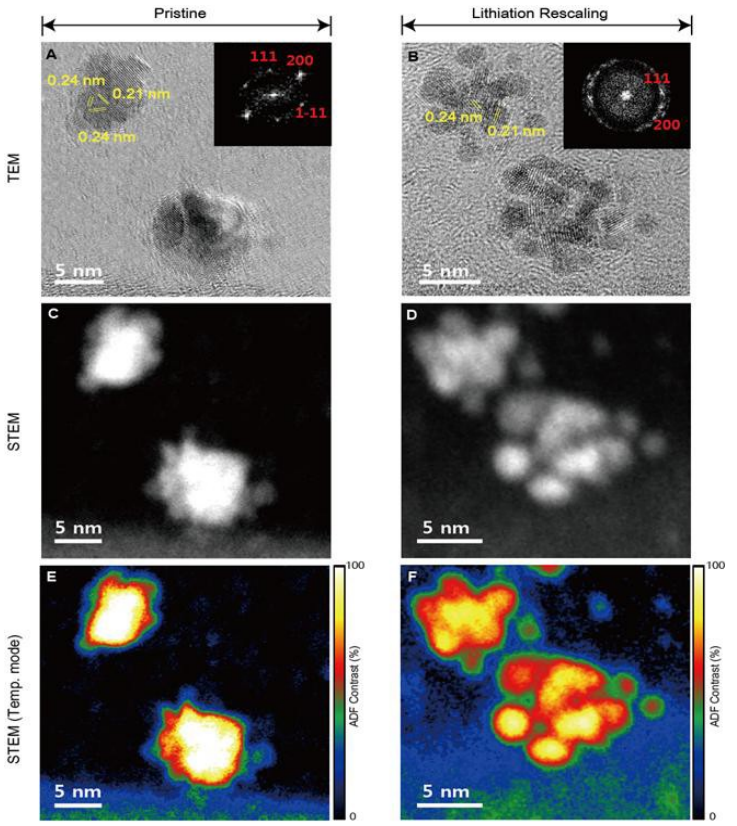

Fig. S6. Cs-TEM & STEM Characterization of a 10-nm NiO particle before and after lithiation-induced rescaling. (*A* and *B*) The HR-TEM image of a 10-nm NiO (*A*) before and (*B*) after rescaling. The yellow markers show the lattice spacing of a NiO nanocrystal. The top right inset shows a FFT diffraction pattern obtained from the NiO nanocrystal. (*C* and *D*) The STEM mapping image of the 10-nm NiO (*C*) before and (*D*) after rescaling at the same spot determined by the TEM. (*E* and *F*) The STEM mapping image (color scale) of the 10-nm NiO (*E*) before and (*F*) after rescaling at the same spot determined by the TEM.

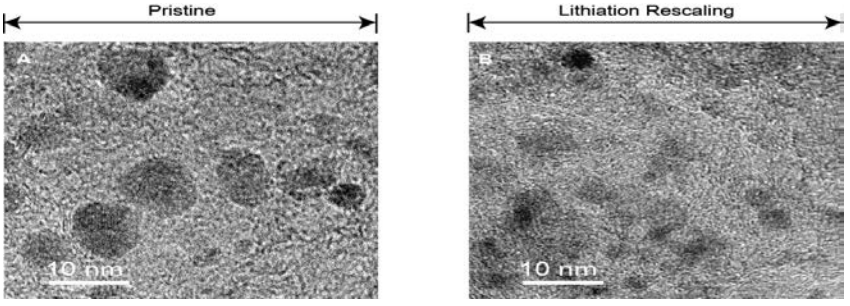

Fig. S7. Ex situ TEM of NiO particles on graphene before and after a slow-rate (6 days) for the rescaling process. The TEM images of 10-nm NiO particles on graphene (*A*) before and (*B*) after the slow-rate rescaling.

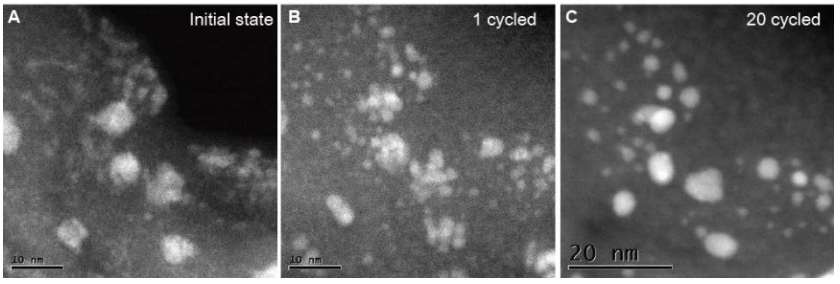

Fig. S8. Ex situ STM of 10-nm NiO particles on graphene before and after the 1 cycle and the 20 cycles for rescaling. The STEM images of 10-nm NiO particles on graphene (*A*) before, (*B*) after the 1 cycle, and (*C*) after the 20 cycles.

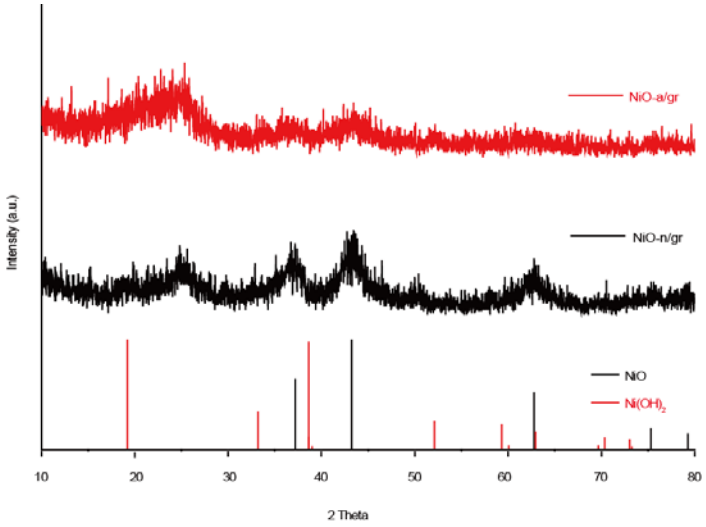

Fig. S9. The PXRD data of 10 nm NiO and rescaled NiO on graphene. The diffraction pattern of NiO-g (black line) is well matched with the standard NiO diffraction pattern (JPCD number 71-1179). After rescaling, the NiO structure remains, although it is broadened due to reduced size. The peak around 25° can be ascribed to graphitic carbon.

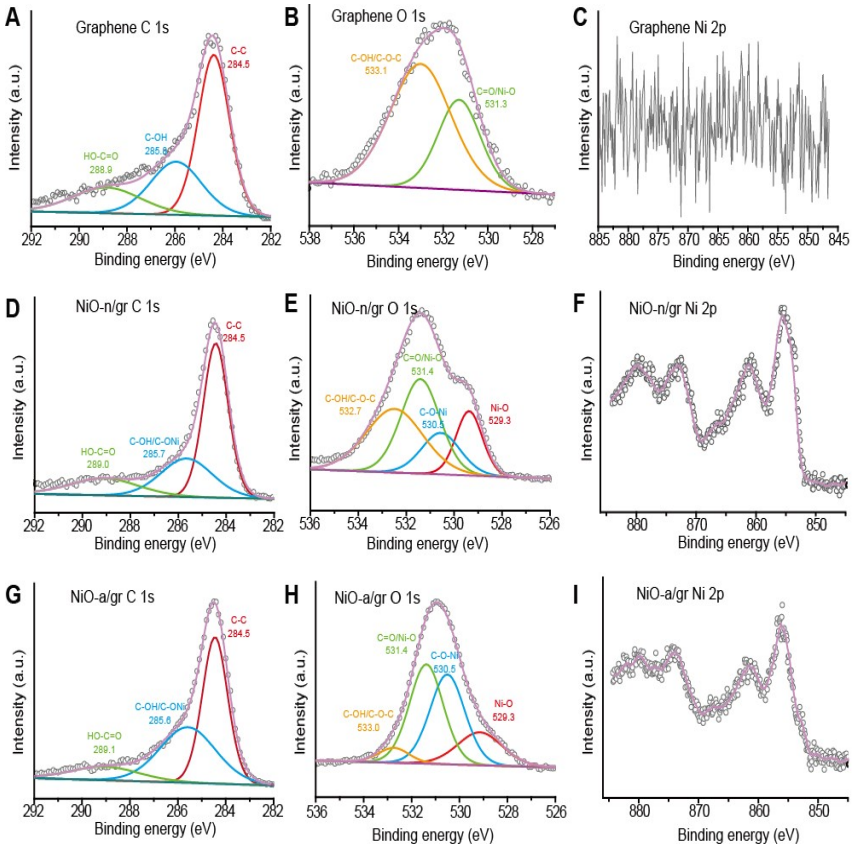

Fig. S10. The XPS spectra of graphene, NiO-n/gr, and NiO-a/gr. (*A*) C 1s, (*B*) O 1s, and (*C*) Ni 2p spectra of graphene. (*D*) C 1s, (*E*) O 1s, and (*F*) Ni 2p spectra of NiO-n/gr. (*G*) C 1s, (*H*) O1s, and (*I*) Ni 2p spectra of NiO-a/gr. Comparing the O 1s spectra, the C-O-Ni linkage between NiO and graphene is increased after rescaling. These results suggests that the rescaled NiO particles are anchored on the oxygenated graphene without transforming into $Ni(OH)_2$.

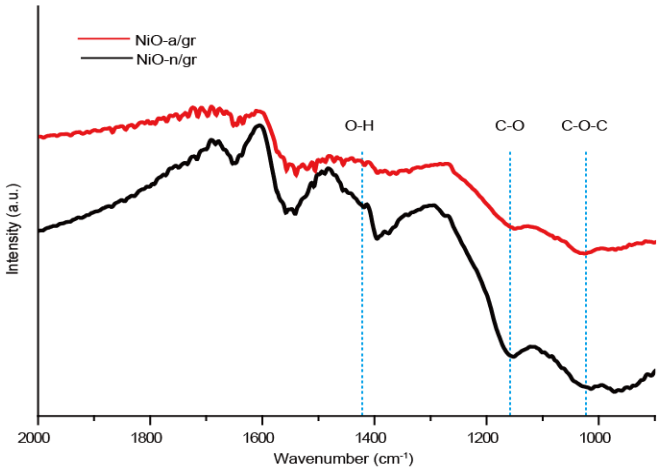

Fig. S11. The FTIR spectra of NiO-n/gr and NiO-a/gr. The binding between the graphene and NiO particles was analyzed by FTIR. The characteristic peaks for the graphene at 1421, 1162, and 1025 cm^{-1} are attributed to the O-H and C-O vibration modes of C-OH groups, and the C-O-C vibration mode of epoxy groups (4-6). It is found that the intensities of these 1421, 1162, and 1025 cm^{-1} peaks are decreased after the rescaling process, thus showing that residual oxygen containing groups on the graphene in NiO-g are broken and form additional C-O-Ni bonds during the rescaling process. An absorption band appears at 1561 cm^{-1}, which is attributed to the skeletal vibration of the graphene sheets (7). Also, the absorption band at 1650 cm^{-1} is assigned to the bending vibration mode of O-H groups from absorbed water molecules (1).

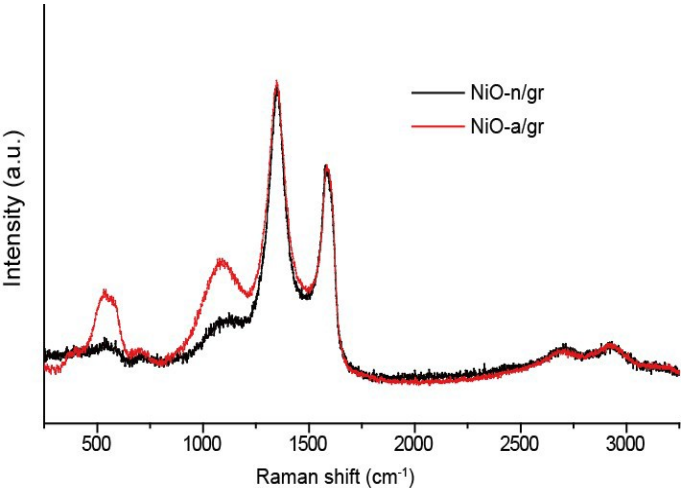

Fig. S12. The Raman spectra of 10 nm NiO and rescaled NiO on graphene. Raman spectra of NiO and rescaled NiO on graphene. In case of the spectra for rescaled NiO on graphene, the intensity of the first longitudinal optical (547 cm^{-1}) and the second longitudinal optical (1100 cm^{-1}) of NiO are increased after the rescaling process, which is attributed to dispersion of rescaled NiO particles. On the other hand, the D and G peaks for the graphene located at 1350 and 1581 cm^{-1} are not changed significantly. The D/G ratio of 1.38 for NiO on graphene (1.38) and the 1.39 for rescaled NiO on graphene are similar.

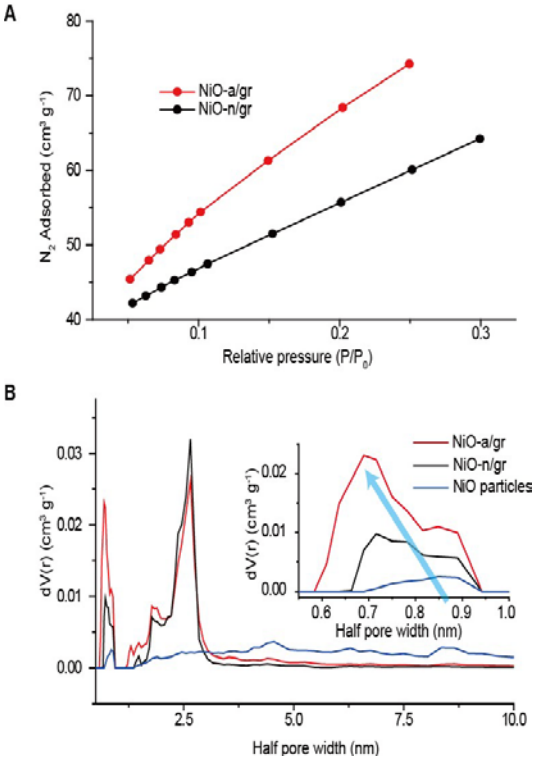

Fig. S13. The N_2 adsorption/desorption measurement of NiO-n/gr and NiO-a/gr. (*A*) the N2 adsorption of NiO-n/gr and NiO-a/gr in the linear region. (*B*) The pore size distributions of NiO particles for NiO-n/gr and NiO-a/gr by the NLDFT method. Peaks at around 2.5 nm originate from the graphene inter-layer of NiO-n/gr and NiO-a/gr are not changed significantly, while pores with less than 1 nm size are increased after rescaling process (inset).

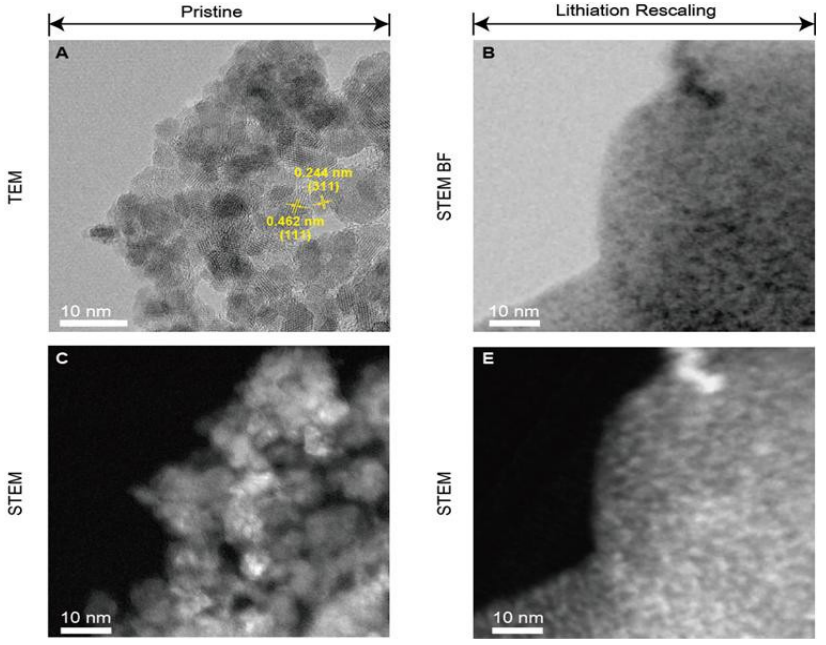

Fig. S14. TEM & STEM Characterizations of cobalt oxide particles before and after lithiation-induced rescaling. (*A*) HR-TEM image of Co_3O_4 particles before rescaling. The yellow markers show the lattice spacing of a Co_3O_4 nanocrystal. (*B*) Bright field (BF) TEM image of lithiation-rescaled Co_3O_4 particles (*C* and *D*) The high angle annular dark field (HAADF) STEM mapping image of the Co_3O_4 particles (*C*) before and (*D*) after rescaling at the same spot examined by TEM.

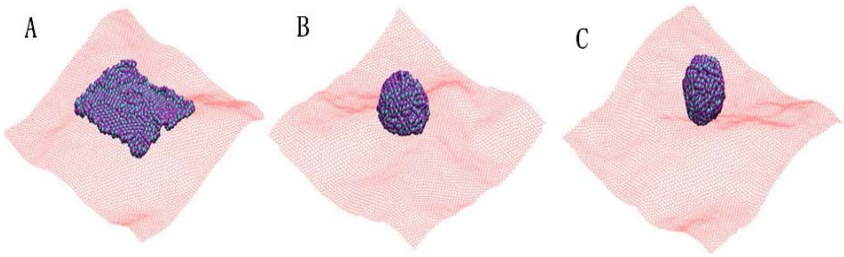

Fig. S15. Three initial structures using in the reactive molecular dynamics simulations to determine most stable form of the NiO nanostructure on graphene. (*A*) NiO monolayer on the top of graphene sheet. Here, the NiO monolayer was built from experimental crystal structure (Fm3m) (100) surface. The length in x and y dimension is 11.8 nm, which consists of 848 atoms (424 Ni and 424 O). This same number of atoms in a NiO semi-sphere has a diameter of 3.0 nm. (*B*) a diameter of 2.38 nm in a NiO sphere. (*C*) The dimensions of the graphene sheet are 14.7 × 13.6 nm^2, which consists of 7,680 carbon atoms. The total system consists of 8,528 atoms. The colors are: C in pink, Ni in silver blue, O in purple.

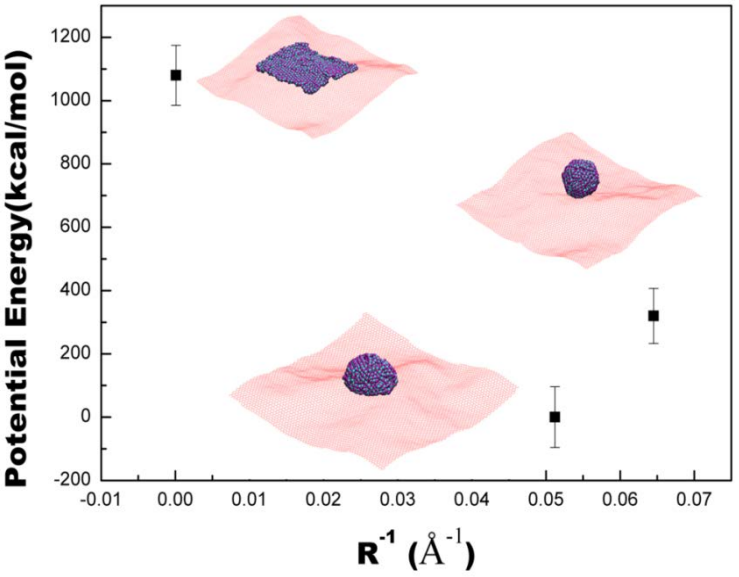

Fig. S16. Comparison of the average potential among three initial models (Fig. S13) during 200 ps NVT simulation at 300 K. X-axis is the curvature (1/R) of NiO clusters: 0.0 for monolayer model, 0.051 for semi-sphere (or cap) model and 0.064 for sphere model, as shown in the insets. Cap model has the lowest potential energy. The sphere model is ~300 kcal/mol higher, and the monolayer structure has the highest potential energy ~1100 kcal/mol. The colors are C in pink, Ni in silver blue, O in purple, the same as Fig. S15.

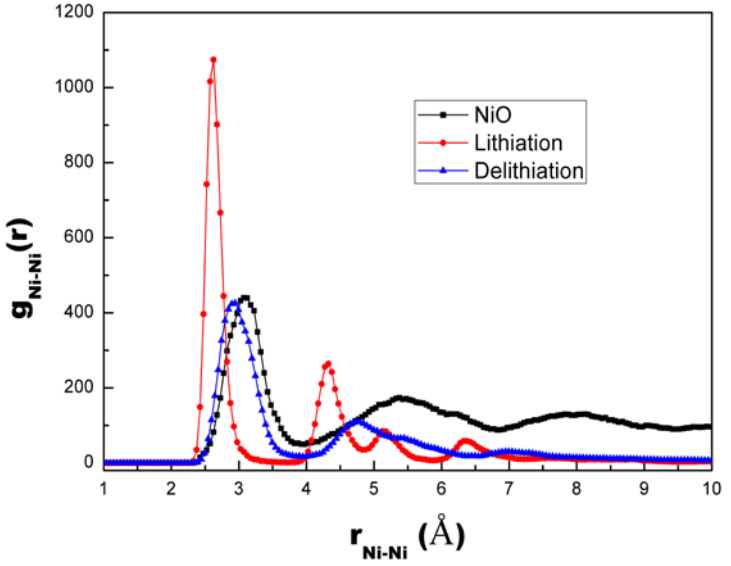

Fig. S17. Comparison for the radial distribution function of gNi-Ni(r) as a function of Ni-Ni distance during different stages of simulation: starting cap model (NiO), after lithiation and after delithiation. The experimental Ni-Ni distance is 2.440 Å in Ni metal (fcc) and 2.954 Å in NiO crystal (Fm3m). Here the solid black line with squares is a radial distribution for the NiO cap, the red line with circles is one after lithiation, and the blue line with triangles is one after delithiation. The detail peak positions and coordination numbers are shown in Table S2.

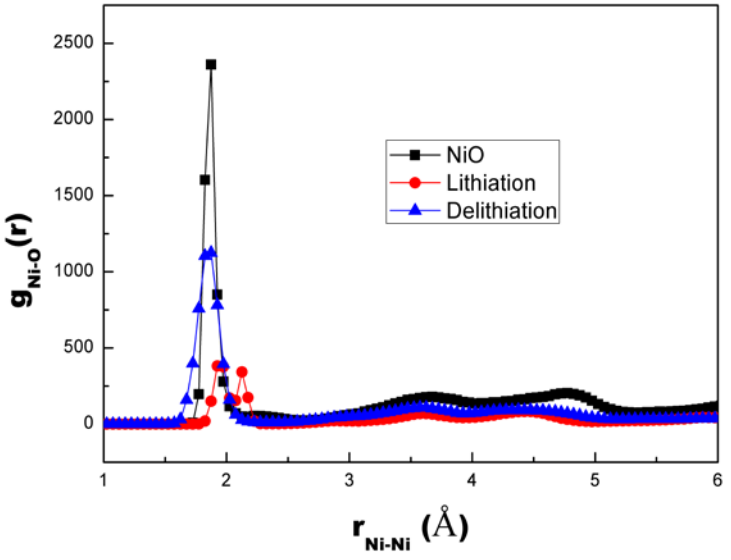

Fig. S18. Comparison for the radial distribution function of gNi-Ni(r) as a function of Ni-Ni distance during different stages of simulation: starting cap model (NiO), after lithiation and after delithiation. The experimental Ni-Ni distance is 2.440 Å in Ni metal (fcc) and 2.954 Å in NiO crystal (Fm3m). Here the solid black line with squares is a radial distribution for the NiO cap, the red line with circles is one after lithiation, and the blue line with triangles is one after delithiation. The detail peak positions and coordination numbers are shown in Table S2.

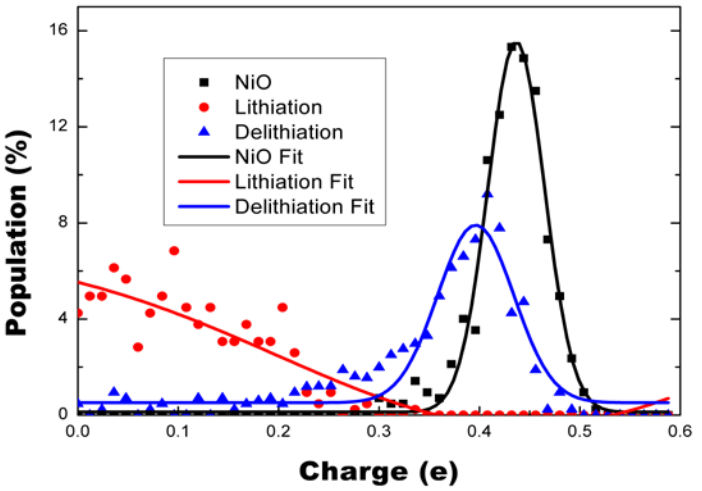

Fig. S19. Comparison of the atomic charge distributions from the RMD simulations of the 3 cases. RMD of NiO (black), RMD on lithiation (blue), and RMD on delithiation (red). The charges (in e) are obtained from the electronegativity equalization method (EEM) implemented in ReaxFF. The parameters in ReaxFF are optimized to fit Mulliken populations in QM, which allows partial covalency. The obtained data were further fitted to Gaussian distribution, which leads to an average charge on Ni of 0.45 for NiO, 0.00 for lithiation and 0.40 for delithiation.

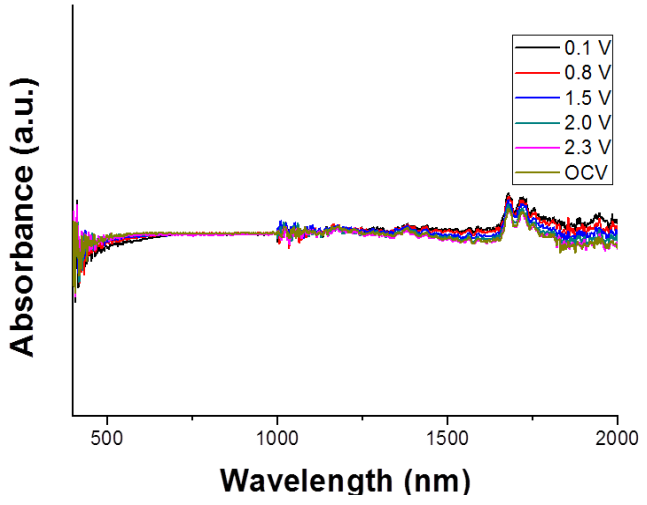

Fig. S20. UV-Vis spectra of the Au-coated substrate at various potentials vs. Li/Li^+. These verify that there is no significant change of the Au thin film by lithiation.

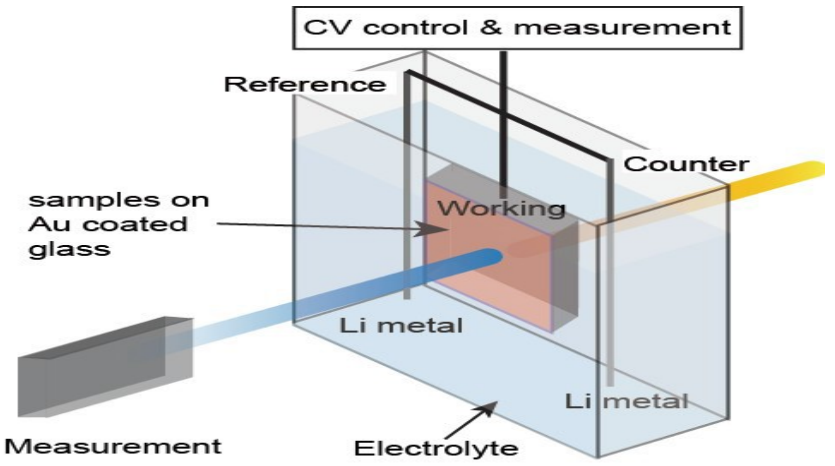

Fig. S21. A scheme diagram of a sepctroelectrochemistry apparatus.

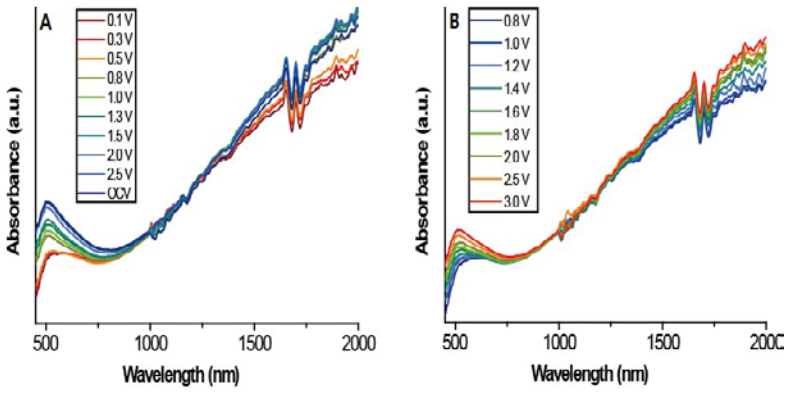

Fig. S22. In situ SEC data of NiO on graphene in the full spectral region. (A) Lithiation. (B) Delithiation.

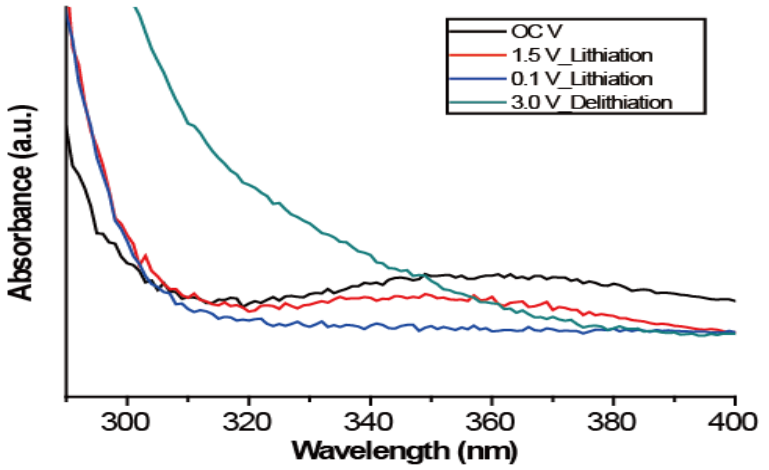

Fig.S23. UV spectra of pure NiO by the ex situ measurement.

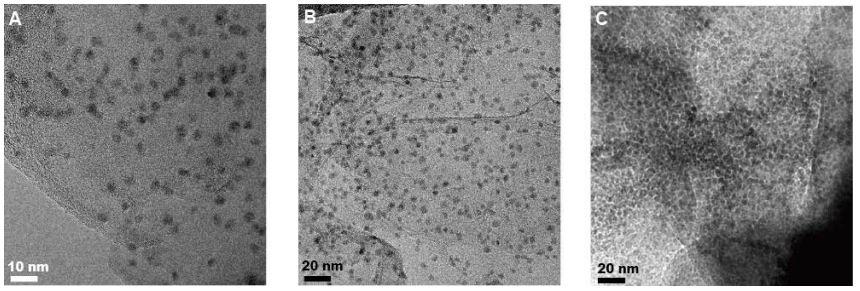

Fig. S24. TEM images of NiO on graphene with 30, 50, and 70 wt. % NiO contents. (*A*) NiO_{30}-n/gr. (*B*) NiO_{50}-n/gr. (*C*) NiO_{70}-n/gr.

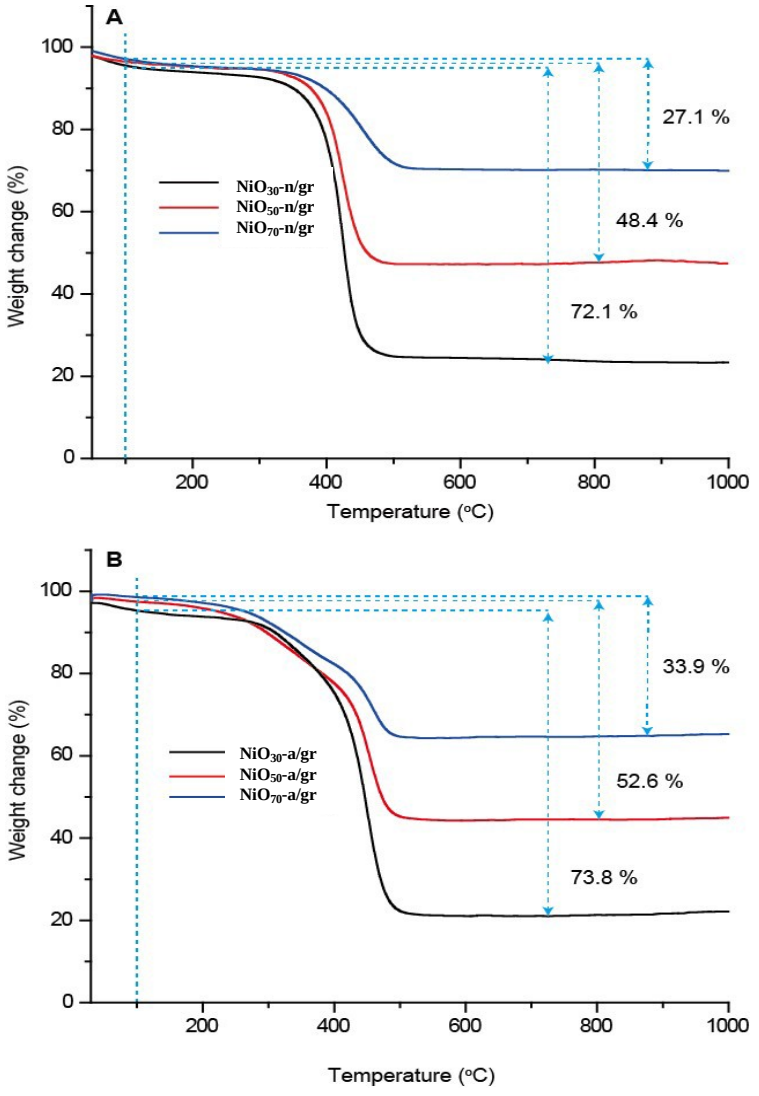

Fig. S25. Thermogravimetric analysis (TGA) measurements for various NiO loadings of (A) NiO-n/gr and (B) NiO-a/gr. (*A*) An apparent large weight loss can be observed at ~500 ˚C and the total amount of the graphene presented in NiO_{30}-n/gr, NiO_{50}-n/gr, and NiO_{70}-n/gr are measured to be 72.1, 51.3, and 27.1 %, respectively. (*B*) After the rescaling process, it was also determined that the graphene contents in NiO_{30}-a/gr, NiO_{50}-a/gr, and NiO_{70}-a/gr are on 73.8 wt. %, 54.2 wt. %, and 33.9 wt. %, respectively. The weight loss of around 2.5 ~ 5 % below 100 ˚C is likely due to evaporation of the absorbed moisture, which is common for materials with a large surface area. The additional plateau located at around 300 ~400 ˚C in TGA data of rescaled samples originates from residual PVDF binder.

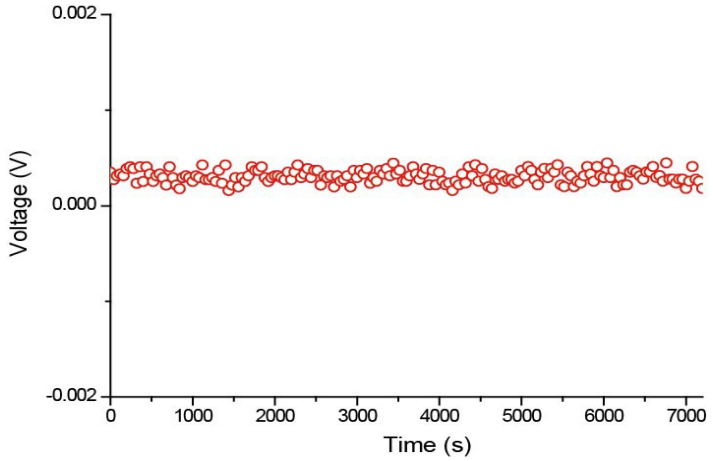

Fig. S26. The open circuit voltage (OCV) measurement between unused Ag/AgCl and used Ag/AgCl reference electrodes after 10,000 cycles. The two Ag/AgCl reference electrodes are used as negative and positive electrode. The voltage difference between two Ag/AgCl reference electrodes is less than 0.0005 V. This difference in value can be disregarded during galvanostatic or CV measurements. Furthermore, in this study, we refreshed the reference electrode at every 10,000 cycles.

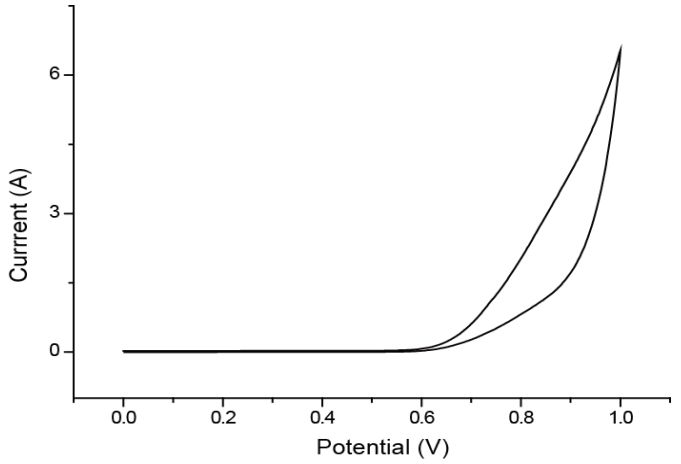

Fig. S27. CV curve of Pt plate as working electrode in a voltage window from 0 to 1 V (vs. Ag/AgCl). There is no reaction in the voltage range from 0 to 0.6 V, while oxygen gas is formed from electrolyte at voltages larger than 0.6 V. This result suggests that the highest voltage allowable for stable operation of a three-electrode cell is up to 0.6 V.

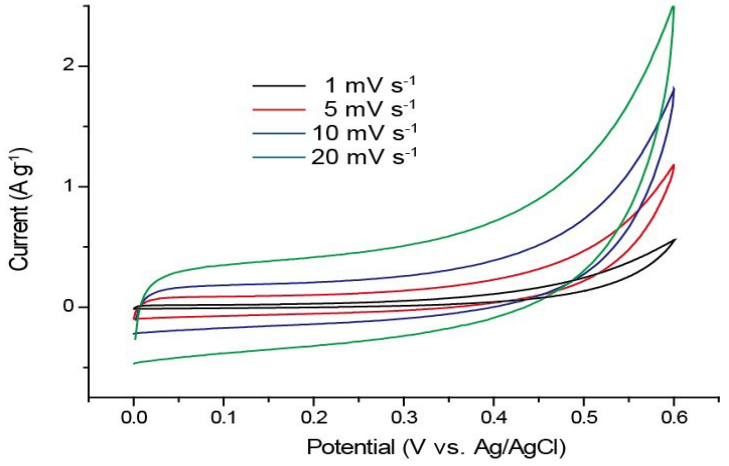

Fig. S28. CV data of NiO-free graphene electrodes at different scan rates.

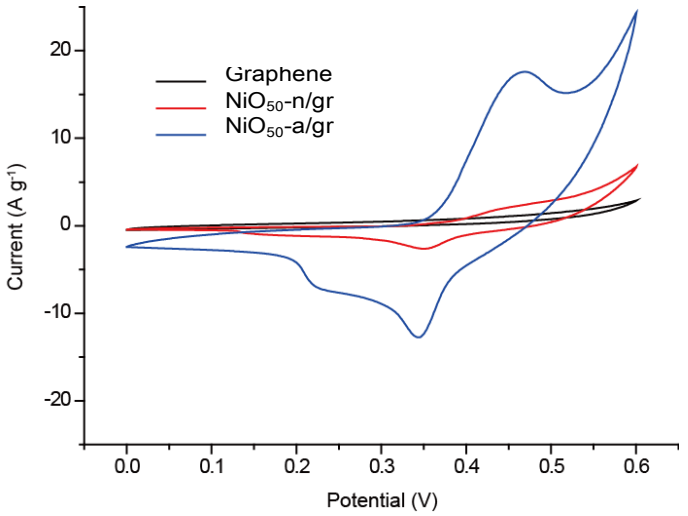

Fig. S29. The voltage profile of NiO on graphene at the first cycle under lithiation rescaling. The plateaus located at around 0.5 V for the discharge curve and at around 1.3 V and 2.3 V for the charge curve of the voltammetry measurements correspond with cathodic and anodic peaks.

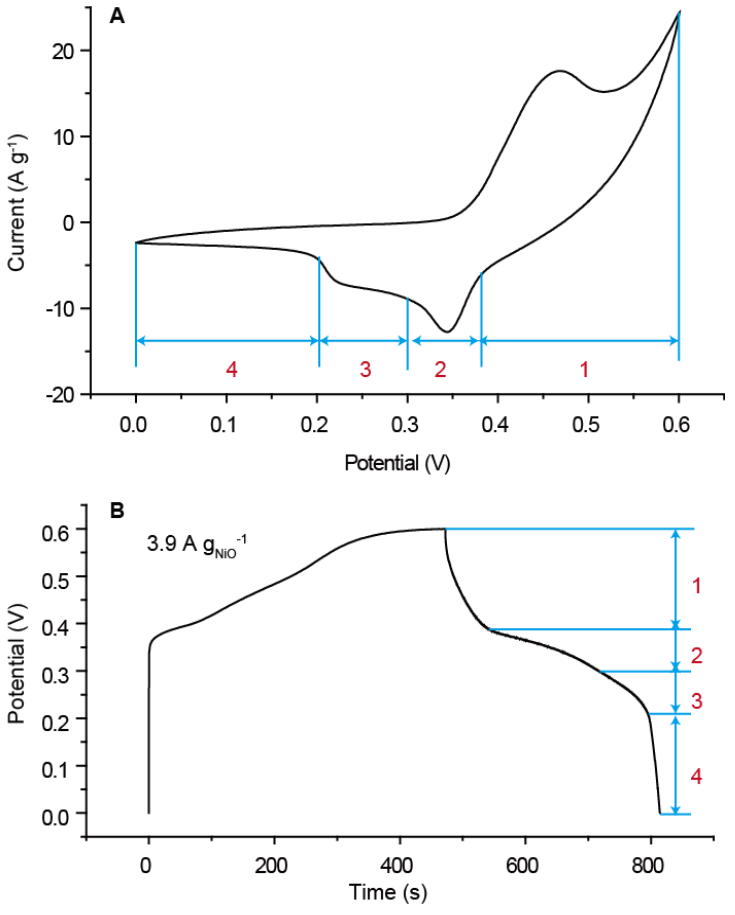

Fig. S30. Comparison of the CV data and the discharge profile of NiO_{50}-a/gr. (*A*) The CV curve of NiO_{50}-a/gr. (*B*) The galvanostatic charge/discharge profile of NiO-a/gr. In comparing the CV data with the charge/discharge profile, each anodic peak, which are numbered as 1 to 4 in the CV curve, is well matched with the corresponding numbered region in the discharge profile.

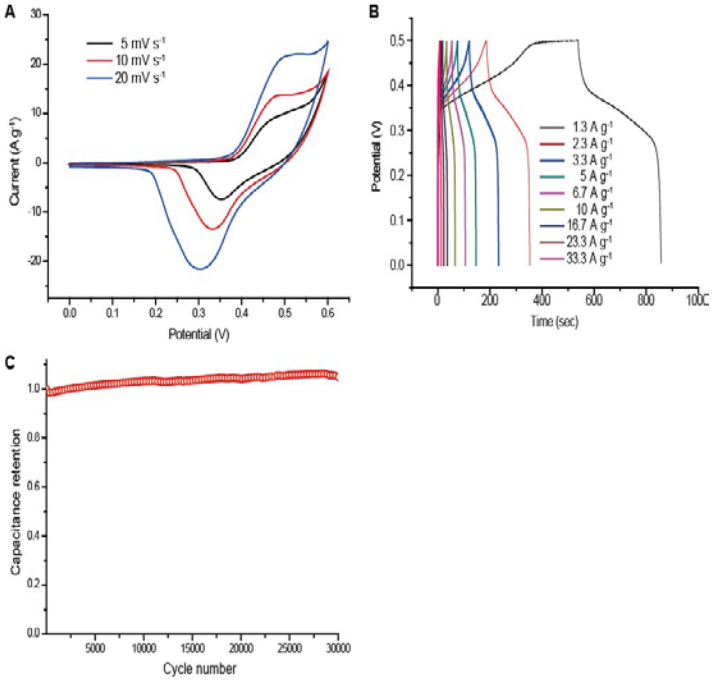

Fig. S31. The electrochemical performance of NiO_{30}-a/gr. (*A*) CV measurements of NiO_{30}-a/gr at various scan rates. (*B*) Charge/discharge profiles measured by galvanostatic characterization at various current densities. (*C*) Cycling test of NiO_{30}-a/gr at a current density of 23.3 A g^{-1}.

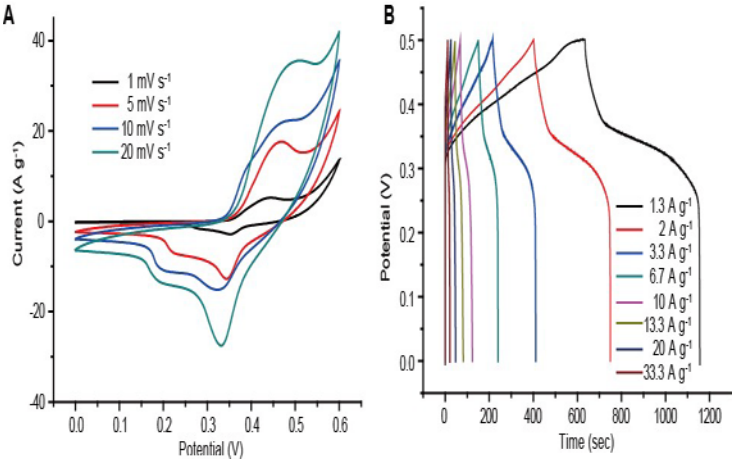

Fig. S32. The electrochemical performance of NiO_{50}-a/gr. (*A*) CV measurements of NiO_{50}-a/gr at various scan rates. (*B*) Charge/discharge profiles measured by galvanostatic characterization at various current densities.

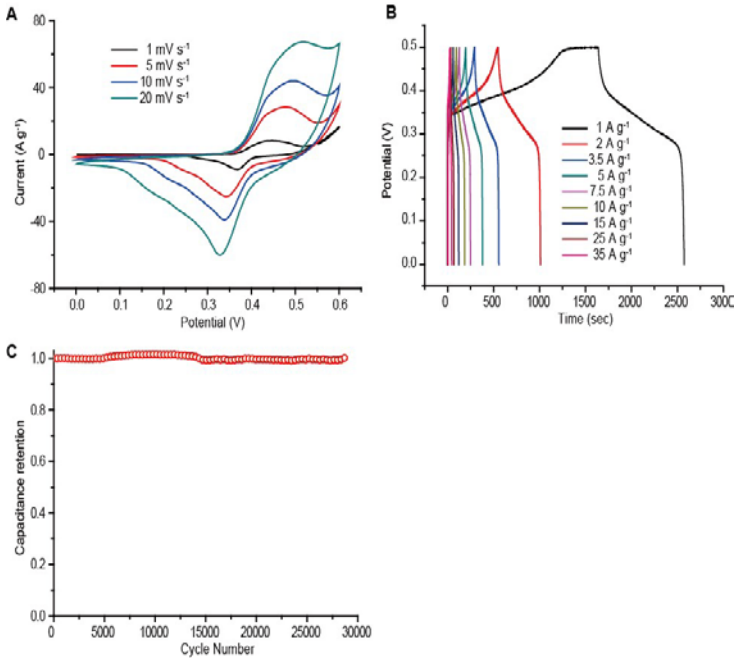

Fig. S33. The electrochemical performance of NiO_{70}-a/gr. (*A*) CV measurements of NiO_{70}-gr at various scan rates. (*B*) Charge/discharge profiles measured by galvanostatic characterization at various current densities. (*C*) Cycling test of NiO_{70}-a/gr at a current density of 25 A g^{-1}.

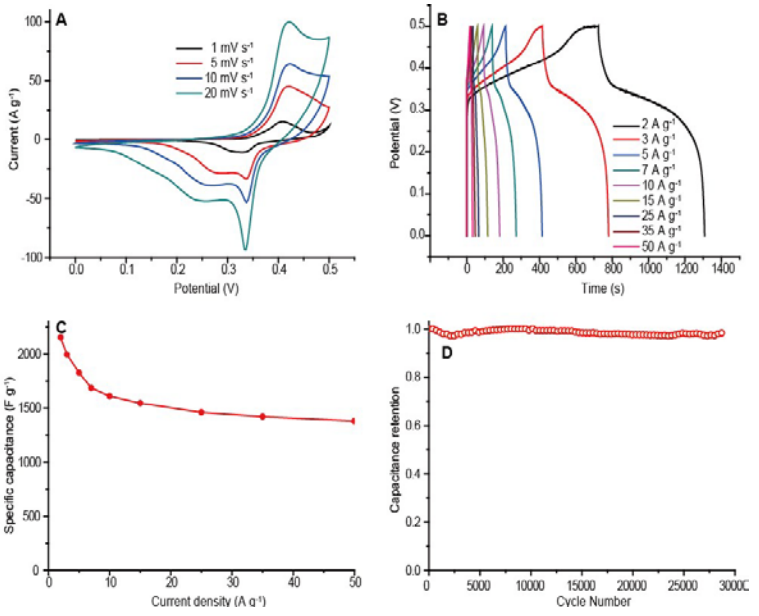

Fig. S34. The electrochemical performance of NiO_{70}-a/gr by using a saturated calomel electrode as a reference. (*A*) CV measurements of NiO_{70}-a/gr at various scan rates. (*B*) Charge/discharge profiles measured by galvanostatic characterization at various current densities. (*C*) Gravimetric capacitance of NiO_{70}-a/gr measured at a series of current density. The capacitance of 2,151 F per the total composite mass at 2 A g^{-1} is comparable to the measured capacitance using a Ag/AgCl reference electrode. (*D*) Cycling test of NiO_{70}-a/gr using a SCE reference electrode.

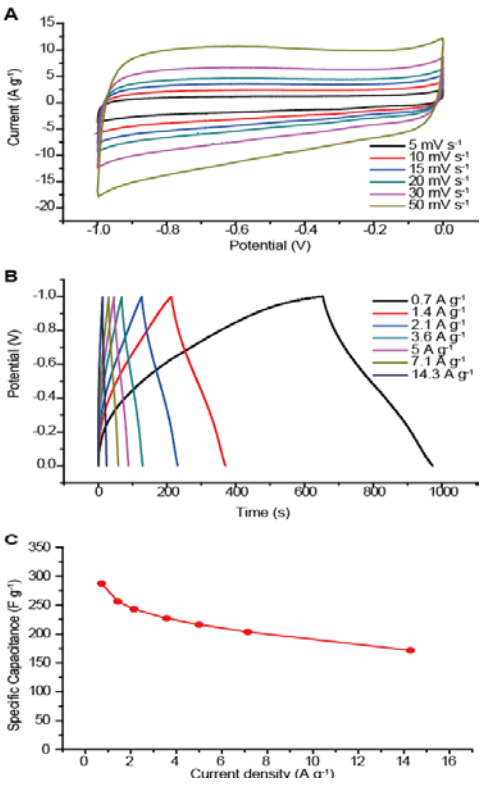

Fig. S35. Electrochemical properties of nitrogen-doped graphene (NG) as a negative electrode for an asymmetric supercapacitor. (*A*) CV measurements of NG at various scan rates. The specific capacitance of NG is 285 F g^{-1} at scan rate of 5 mV s^{-1}. (*B*) Charge/discharge profiles measured by galvanostatic characterization at various current densities. (*C*) Gravimetric capacitance of NG measured at a series of current densities. The electrochemical performance is measured using 1 M KOH aqueous electrolyte, a Ag/AgCl reference electrode, and a platinum wire counter electrode.

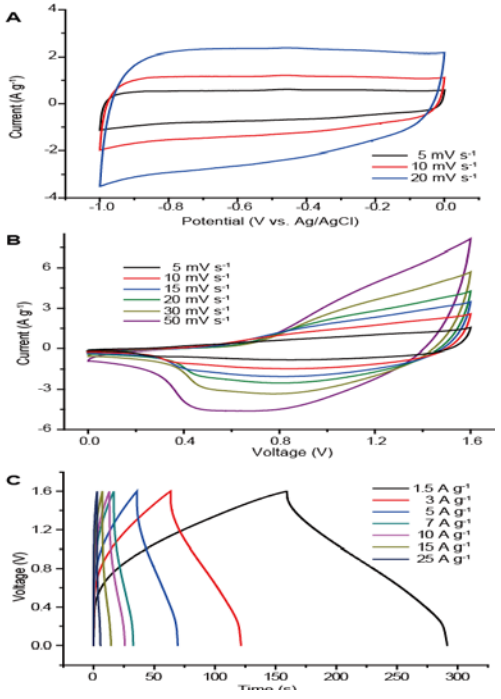

Fig. S36. Electrochemical properties of the activated carbon (AC) as a negative electrode and the NiO_{70}-a/gr||AC asymmetric capacitor. (*A*) CV measurements of the AC negative electrode at various scan rates. The specific capacitance of AC is 122 F g^{-1} at scan rate of 5 mV s^{-1}. (*B*) CV measurements of the NiO-a/gr||AC asymmetric capacitor at various scan rates. The two redox peaks indicate the pseudo-capacitive property. (*C*) Charge- discharge profile of the NiO-a/gr||AC asymmetric capacitor measured by galvanostatic characterizations at various current densities.

SI Table

Table S1. The ReaxFF parameters in the format for LAMMPS. Reactive MD-force field

```
39 ! Number of general parameters
50.0000 !Comment here
9.5469 !Comment here
26.5405 !Comment here
1.7224 !Comment here
6.8702 !Comment here
60.4850 !Comment here
1.0588 !Comment here
4.6000 !Comment here
12.1176 !Comment here
13.3056 !Comment here
-70.5044 !Comment here
0.0000 !Comment here
10.0000 !Comment here
2.8793 !Comment here
33.8667 !Comment here
6.0891 !Comment here
1.0563 !Comment here
2.0384 !Comment here
6.1431 !Comment here
6.9290 !Comment here
0.3842 !Comment here
2.9294 !Comment here
-2.4837 !Comment here
5.7796 !Comment here
10.0000 !Comment here
1.9487 !Comment here
-1.2327 !Comment here
2.1645 !Comment here
1.5591 !Comment here
0.1000 !Comment here
2.1365 !Comment here
0.6991 !Comment here
50.0000 !Comment here
1.8512 !Comment here
0.5000 !Comment here
20.0000 !Comment here
5.0000 !Comment here
0.0000 !Comment here
2.6962 !Comment here

11      !Nr of atoms; cov.r; valency;a.m;Rvdw;Evdw;gammaEEM;cov.r2;
alfa;gammavdW;valency;Eunder;Eover;chiEEM;etaEEM;n.u. cov r3;Elp;Heat inc.;n.u.;n.u.;n.u.;n.u.
ov/un;val1;n.u.;val3,vval4

C       1.3831    4.0000   12.0000   1.8814    0.1923    0.9000    1.1363    4.0000
        9.7821    2.1317    4.0000   30.0000   79.5548    5.9666    7.0000    0.0000
        1.2071    0.0000  186.1720    9.0068   34.9357   13.5366    0.8563    0.0000
       -2.8983    2.5675    1.0564    4.0000    2.9663    0.0000    0.0000    0.0000
H       0.8873    1.0000    1.0080    1.5420    0.0598    0.6883   -0.1000    1.0000
        8.1910   30.9706    1.0000    0.0000  121.1250    3.5768   10.5896    1.0000
       -0.1000    0.0000   54.0596    1.3986    2.1457    0.0003    1.0698    0.0000
      -15.7683    2.1488    1.0338    1.0000    2.8793    0.0000    0.0000    0.0000
O       1.2450    2.0000   15.9990    2.3878    0.1023    1.0903    1.0548    6.0000
       10.5750   32.3923    4.0000   37.5000  116.0768    8.5000    7.5600    2.0000
        0.9049   -1.0100   70.1357    2.7162    3.2532    0.0021    0.9745    0.0000
       -3.6141    2.7025    1.0493    4.0000    2.9225    0.0000    0.0000    0.0000
N       1.2333    3.0000   14.0000    1.9324    0.1376    0.8596    1.1748    5.0000
       10.0667    7.8431    4.0000   32.2482  100.0000    6.8418    6.3404    2.0000
        1.0433   13.7673  139.9837    2.1961    3.0696    2.7683    0.9745    0.0000
       -4.3875    2.6192    1.0183    4.0000    2.8793    0.0000    0.0000    0.0000
S       1.9405    2.0000   32.0600    2.0677    0.2099    1.0336    1.5479    6.0000
        9.9575    4.9055    4.0000   52.9998  112.1416    5.6210    8.2545    2.0000
        1.4601    9.7177   71.1843    5.7487   23.2859   12.7147    0.9745    0.0000
      -11.0000    2.7466    1.0338    6.2998    2.8793    0.0000    0.0000    0.0000
F       1.2100    1.0000   18.9984    1.8601    0.1200    0.3000   -0.1000    7.0000
       11.5000    7.5000    4.0000    9.2533    0.2000    9.0000   15.0000    0.0000
       -1.0000   35.0000   33.1268    6.9821    4.1799    1.0561    0.0000    0.0000
       -7.3000    2.6656    1.0493    4.0000    2.9225    0.0000    0.0000    0.0000
Pt      1.9820    2.0000  195.0800    2.0423    0.3309    0.3738   -1.0000    2.0000
       12.3677    6.0083    2.0000    0.0000    0.0000    5.6538    6.2512    0.0000
       -1.0000    0.0000  142.6300   26.2350    3.2757    0.1586    0.8563    0.0000
      -13.0000    1.7934    1.0338    5.0000    2.5791    0.0000    0.0000    0.0000
Cl      1.8500    1.0000   35.4500    2.0155    0.2300    0.8218   -1.0000    7.0000
       11.5000    8.1330    1.0000    0.0000    0.0000    8.5038    8.0852    0.0000
       -1.0000    0.0000   42.6300    6.2293    5.2294    0.1542    0.8563    0.0000
      -10.2080    2.9867    1.0338    1.0000    2.5791    0.0000    0.0000    0.0000
```

Ni	1.8201	2.0000	58.6900	1.9449	0.1880	0.8218	0.1000	2.0000
	12.1594	3.8387	2.0000	0.0000	0.0000	4.8038	7.3852	0.0000
	-1.0000	0.0000	95.6300	50.6786	0.6762	0.0981	0.8563	0.0000
	-3.7733	3.6035	1.0338	8.0000	2.5791	0.0000	0.0000	0.0000
Li	2.3000	1.0000	6.9410	1.8913	0.1987	0.5722	-0.1000	1.0000
	10.8525	2.1866	1.0000	0.0000	0.0000	-2.9334	10.4936	0.0000
	-1.0000	0.0000	37.5000	5.4409	6.9107	0.1973	0.8563	0.0000
	-2.5000	2.2989	1.0338	1.0000	2.8103	0.0000	0.0000	0.0000
X	-0.1000	2.0000	1.0080	2.0000	0.0000	1.0000	-0.1000	6.0000
	10.0000	2.5000	4.0000	0.0000	0.0000	8.5000	1.5000	0.0000
	-0.1000	0.0000	-2.3700	8.7410	13.3640	0.6690	0.9745	0.0000
	-11.0000	2.7466	1.0338	4.0000	2.8793	0.0000	0.0000	0.0000

43 ! Nr of bonds; Edis1;LPpen;n.u.;pbe1;pbo5;13corr;pbo6;
pbe2;pbo3;pbo4;n.u.;pbo1;pbo2;ovcorr

1	1 143.3883		96.3926	76.4404	-0.7767	-0.4710	1.0000	34.9900	0.5108
	0.4271	-0.1116	9.0638	1.0000	-0.0840	6.7452	1.0000	0.0000	
1	2 181.9084		0.0000	0.0000	-0.4768	0.0000	1.0000	6.0000	0.7499
	12.8085	1.0000	0.0000	1.0000	-0.0608	6.9928	0.0000	0.0000	
1	3	158.6946	107.4583	23.3136	-0.4240	-0.1743	1.0000	10.8209	1.0000
		0.5322	-0.3113	7.0000	1.0000	-0.1447	5.2450	0.0000	0.0000
1	4	134.1215	140.2179	79.9745	0.0163	-0.1428	1.0000	27.0617	0.2000
		0.1387	-0.3681	7.1611	1.0000	-0.1000	5.0825	1.0000	0.0000
1	5	128.7959	56.4134	39.0716	0.0688	-0.4463	1.0000	31.1766	0.4530
		0.1955	-0.3587	6.2148	1.0000	-0.0770	6.6386	1.0000	0.0000
1	6	237.8781	0.0000	0.0000	-0.7438	-0.5000	1.0000	35.0000	1.0460
		3.6661	-0.2500	15.0000	1.0000	-0.0800	5.4719	1.0000	0.0000
1	7	164.4424	0.0000	0.0000	-0.0754	-0.2000	1.0000	16.0000	0.4351
		0.9325	-0.2000	15.0000	1.0000	-0.1809	7.3578	1.0000	0.0000
1	8	50.6675	0.0000	0.0000	0.0004	-0.2000	0.0000	16.0000	0.3115
		1.0000	-0.2000	15.0000	1.0000	-0.1062	5.1596	0.0000	0.0000
1	9	83.5810	9.0383	0.0000	0.2531	-0.2000	1.0000	16.0000	0.0529
		1.4085	-0.1113	13.3900	1.0000	-0.1436	4.5683	1.0000	0.0000
1	10	47.4101	-0.0200	0.0000	1.0000	-0.5000	0.0000	35.0000	0.7328
		1.0000	-0.2500	11.9965	1.0000	-0.1141	9.1243	0.0000	0.0000
2	2	168.2342	0.0000	0.0000	-0.2191	0.0000	1.0000	6.0000	1.0062
		6.1152	1.0000	0.0000	1.0000	-0.0889	6.0000	0.0000	0.0000
2	3	163.1043	0.0000	0.0000	-0.4155	0.0000	1.0000	6.0000	0.3607
		1.9380	1.0000	0.0000	0.0000	-0.0778	4.3082	0.0000	0.0000
2	4	231.8173	0.0000	0.0000	-0.3364	0.0000	1.0000	6.0000	0.4402
		8.8910	1.0000	0.0000	1.0000	-0.0327	6.5754	0.0000	0.0000
2	5	136.1049	0.0000	0.0000	-0.4669	0.0000	1.0000	6.0000	0.3803
		10.5730	1.0000	0.0000	1.0000	-0.1000	7.0000	1.0000	0.0000
2	6	0.0000	0.0000	0.0000	-0.4643	0.0000	1.0000	6.0000	0.6151
		12.3710	1.0000	0.0000	1.0000	-0.1008	8.5980	0.0000	0.0000
2	7	158.0215	0.0000	0.0000	-0.2597	0.0000	1.0000	6.0000	0.2532
		36.8276	1.0000	0.0000	1.0000	-0.0837	10.5233	0.0000	0.0000
2	8	50.6675	0.0000	0.0000	0.0004	-0.2000	0.0000	16.0000	0.3115
		1.0000	-0.2000	15.0000	1.0000	-0.1062	5.1596	0.0000	0.0000
2	9	114.7566	0.0000	0.0000	-0.8939	0.0000	1.0000	6.0000	0.1256
		0.1054	1.0000	0.0000	1.0000	-0.1196	5.0815	0.0000	0.0000
3	3	200.0000	230.7321	50.8293	0.2506	-0.1000	1.0000	29.7503	0.6051
		0.3451	-0.1055	9.0000	1.0000	-0.1225	5.5000	1.0000	0.0000
3	4	130.8596	169.4551	40.0000	0.3837	-0.1639	1.0000	35.0000	0.2000
		1.0000	-0.3579	7.0004	1.0000	-0.1193	6.8773	1.0000	0.0000
3	5	165.3308	220.0000	40.0000	0.7131	-0.2406	1.0000	22.1005	0.2000
		0.8027	-0.2748	8.3393	1.0000	-0.1043	5.6108	1.0000	0.0000
3	6	0.0000	0.0000	0.0000	0.2500	-0.5000	1.0000	45.0000	0.6000
		0.4000	-0.2500	15.0000	1.0000	-0.1000	10.0000	1.0000	0.0000
3	7	184.0448	0.0000	0.0000	-0.6623	-0.2000	1.0000	16.0000	0.0151
		0.6439	-0.2000	15.0000	1.0000	-0.1422	5.0000	1.0000	0.0000
3	8	50.6675	0.0000	0.0000	0.0004	-0.2000	0.0000	16.0000	0.3115
		1.0000	-0.2000	15.0000	1.0000	-0.1062	5.1596	0.0000	0.0000
3	9	118.6999	0.0000	0.0000	-0.1042	-0.2000	0.0000	16.0000	0.1724
		0.8280	-0.2500	15.0000	1.0000	-0.1013	5.6326	1.0000	0.0000
3	10	72.4912	0.4651	0.0000	-1.6243	0.3000	1.0000	6.0000	0.3364
		0.7082	-0.2500	11.9965	1.0000	-0.0512	5.4218	1.0000	0.0000
4	4	157.9384	82.5526	152.5336	0.4010	-0.1034	1.0000	12.4261	0.5828
		0.1578	-0.1509	11.9186	1.0000	-0.0861	5.4271	1.0000	0.0000
4	5	130.0000	180.0000	0.0000	0.5000	-0.2000	1.0000	40.0000	0.3000
		0.4000	-0.2500	9.0000	1.0000	-0.1000	6.0000	1.0000	0.0000
4	6	0.0000	0.0000	0.0000	-0.4643	0.0000	1.0000	6.0000	0.6151
		12.3710	1.0000	0.0000	1.0000	-0.0098	8.5980	0.0000	0.0000
4	7	183.3242	0.0000	0.0000	0.5441	-0.2000	1.0000	16.0000	0.6888
		-0.0634	-0.2000	15.0000	1.0000	-0.1558	5.0000	1.0000	0.0000
4	8	50.6675	0.0000	0.0000	0.0004	-0.2000	0.0000	16.0000	0.3115
		1.0000	-0.2000	15.0000	1.0000	-0.1062	5.1596	0.0000	0.0000
5	5	96.1871	93.7006	68.6860	0.0955	-0.4781	1.0000	17.8574	0.6000
		0.2723	-0.2373	9.7875	1.0000	-0.0950	6.4757	1.0000	0.0000
5	6	0.0000	0.0000	0.0000	0.2500	-0.5000	1.0000	45.0000	0.6000
		0.4000	-0.2500	15.0000	1.0000	-0.1000	10.0000	1.0000	0.0000
5	7	0.0000	0.0000	0.0000	0.2500	-0.5000	1.0000	45.0000	0.6000
		0.4000	-0.2500	15.0000	1.0000	-0.1000	10.0000	1.0000	0.0000
6	6	250.0765	0.0000	0.0000	0.2298	-0.3500	1.0000	25.0000	0.8427
		0.1167	-0.2500	15.0000	1.0000	-0.1506	7.3516	1.0000	0.0000
6	7	-0.0100	0.0000	0.0000	0.9248	-0.3500	1.0000	35.0000	0.1231
		0.3064	-0.2500	25.0000	1.0000	-0.1903	8.4146	1.0000	0.0000

7	7	122.1369	0.0000	0.0000	-0.3578	-0.2000	0.0000	16.0000	0.2877
		0.9897	-0.2000	15.0000	1.0000	-0.0853	5.4801	0.0000	0.0000
7	8	140.6675	0.0000	0.0000	0.0004	-0.2000	0.0000	16.0000	0.3115
		1.0000	-0.2000	15.0000	1.0000	-0.1062	5.1596	0.0000	0.0000
7	9	68.1705	0.0000	0.0000	0.9869	-0.2000	0.0000	16.0000	0.0100
		0.2118	-0.2000	15.0000	1.0000	-0.2148	4.0000	0.0000	0.0000
8	8	125.6675	0.0000	0.0000	0.0004	-0.2000	0.0000	16.0000	0.3115
		1.0000	-0.2000	15.0000	1.0000	-0.1062	7.0000	0.0000	0.0000
9	9	91.2220	0.0000	0.0000	-0.2538	-0.2000	0.0000	16.0000	0.2688
		1.4651	-0.2000	15.0000	1.0000	-0.1435	4.3908	0.0000	0.0000
9	10	29.8068	0.0000	0.0000	0.0672	0.3000	0.0000	26.0000	0.1516
		0.1593	0.0000	12.0000	1.0000	-0.1000	6.5520	0.0000	0.0000
10	10	27.9380	0.0000	0.0000	1.0000	0.3000	0.0000	26.0000	0.4440
		0.2370	0.0000	12.0000	1.0000	-0.1000	6.5000	0.0000	0.0000

24 ! Nr of off-diagonal terms; Ediss;Ro;gamma;rsigma;rpi;rpi2

1	2	0.1188	1.4017	9.8545	1.1203	-1.0000	-1.0000
1	3	0.1156	1.8520	9.8317	1.2854	1.1352	1.0706
1	4	0.1447	1.8766	9.7990	1.3436	1.1885	1.1363
1	5	0.1408	1.8161	9.9393	1.7986	1.3021	1.4031
1	6	0.1071	1.6243	11.0402	1.3176	-1.0000	-1.0000
1	7	0.1204	1.6025	13.6892	1.8982	-1.0000	-1.0000
1	9	0.0800	1.7085	10.0895	1.5504	1.4005	-1.0000
1	10	0.0313	2.4092	11.1978	1.7384	-1.0000	-1.0000
2	3	0.0299	1.3153	10.9102	0.9093	-1.0000	-1.0000
2	4	0.1059	1.8290	9.7818	0.9598	-1.0000	-1.0000
2	5	0.0895	1.6239	10.0104	1.4640	-1.0000	-1.0000
2	6	0.0431	1.7204	10.3632	0.5386	-1.0000	-1.0000
2	7	0.0920	1.6015	11.1362	1.7404	-1.0000	-1.0000
2	9	0.0366	1.7306	11.1019	1.2270	-1.0000	-1.0000
3	4	0.1048	2.0003	10.1220	1.3173	1.1096	1.0206
3	5	0.2250	1.7911	10.2423	1.4546	1.4011	-1.0000
3	7	0.1042	2.0014	10.3651	1.5000	-1.0000	-1.0000
3	9	0.0504	1.7959	11.7893	1.4423	-1.0000	-1.0000
3	10	0.9021	1.2957	9.4755	1.2430	-1.0000	-1.0000
4	5	0.1505	1.9000	10.5104	1.8000	1.4000	-1.0000
4	7	0.1000	2.0294	12.2593	1.5743	-1.0000	-1.0000
7	8	0.1847	2.1006	11.0261	1.7524	-1.0000	-1.0000
7	9	0.1919	2.1352	12.2879	1.8319	-1.0000	-1.0000
9	10	0.2470	1.5755	11.2778	1.8319	-1.0000	-1.0000

104 ! Nr of angles;at1;at2;at3;Thetao,o;ka;kb;pv1;pv2

1	1	1	72.7917	38.5829	0.7209	0.0000	0.1409	17.4509	1.0670
1	1	2	72.1533	14.2108	6.2512	0.0000	0.0100	0.0000	1.1022
1	1	3	49.6811	7.1713	4.3889	0.0000	0.7171	10.2661	1.0463
1	1	4	66.1305	12.4661	7.0000	0.0000	3.0000	50.0000	1.1880
1	1	5	74.4180	33.4273	1.7018	0.1463	0.5000	0.0000	1.6178
1	1	6	74.0446	35.8484	6.6125	0.0000	0.9453	0.0000	3.0000
1	1	7	47.5496	27.7661	4.1587	0.0000	0.1071	0.0000	2.7036
1	1	9	87.6241	12.6504	1.8145	0.0000	0.6154	0.0000	1.5298
1	2	1	0.0000	7.5000	5.0000	0.0000	0.0000	0.0000	1.0400
1	2	2	0.0000	0.0000	6.0000	0.0000	0.0000	0.0000	1.0400
1	2	3	0.0000	25.0000	3.0000	0.0000	1.0000	0.0000	1.0400
1	2	4	0.0000	0.0019	6.0000	0.0000	0.0000	0.0000	1.0400
1	2	5	0.0000	0.0019	6.0000	0.0000	0.0000	0.0000	1.0400
1	2	7	0.0000	1.0000	0.3609	0.0000	0.2947	0.0000	2.6479
1	2	9	0.0000	0.2811	1.1741	0.0000	0.9136	0.0000	3.8138
1	3	1	73.5312	44.7275	0.7354	0.0000	3.0000	0.0000	1.0684
1	3	2	70.1880	20.9562	0.3864	0.0000	0.0050	0.0000	1.6924
1	3	3	79.4761	36.3701	1.8943	0.0000	0.7351	67.6777	3.0000
1	3	4	82.4890	31.4554	0.9953	0.0000	1.6310	0.0000	1.0783
1	3	5	58.9977	36.2016	1.7948	0.0000	0.4304	0.0000	3.0000
1	3	7	88.1962	49.8841	9.8946	0.0000	3.6749	0.0000	1.1000
1	3	9	70.0000	25.0000	1.0000	0.0000	1.0000	0.0000	1.2500
1	4	1	66.0330	22.0295	1.4442	0.0000	1.6777	0.0000	1.0500
1	4	2	69.1106	25.5067	1.1003	0.0000	0.0222	0.0000	1.0369
1	4	3	103.3204	33.0381	0.5787	0.0000	1.6777	0.0000	1.0500
1	4	4	104.1335	8.6043	1.6495	0.0000	1.6777	0.0000	1.0500
1	5	1	79.7037	28.2036	1.7073	0.1463	0.5000	0.0000	1.6453
1	5	2	85.9449	38.3109	1.2492	0.0000	0.5000	0.0000	1.1000
1	5	3	70.0000	35.0000	3.4223	0.0000	1.3550	0.0000	1.2002
1	5	5	85.6645	40.0000	2.9274	0.1463	0.5000	0.0000	1.3830
1	6	1	0.0000	19.9962	3.2299	0.0000	2.1012	0.0000	1.1537
1	6	6	0.0000	25.0000	1.0000	0.0000	1.0000	0.0000	1.0400
1	7	1	37.5291	7.4679	1.6697	0.0000	1.0031	0.0000	2.2937
1	7	2	80.6353	1.0000	0.2000	0.5000	1.2901	0.0000	1.1404
1	7	3	89.0446	31.3538	3.2706	0.0000	2.2596	0.0000	1.1575
1	7	7	45.9456	1.0000	0.2000	0.0000	0.9740	0.0000	2.9993
1	9	1	62.5000	16.6806	0.7981	0.0000	0.9630	0.0000	1.0711
1	9	2	97.5742	10.9373	2.5200	0.0000	1.8558	0.0000	1.0000
1	9	3	70.0000	25.0000	1.0000	0.0000	1.0000	0.0000	1.2500
1	9	9	5.0994	3.1824	0.7016	0.0000	0.7465	0.0000	2.2665
2	1	2	73.2608	24.9703	3.7807	0.0000	0.1335	0.0000	3.0461
2	1	3	65.0000	13.8815	5.0583	0.0000	0.4985	0.0000	1.4900
2	1	4	74.2929	31.0883	2.6184	0.0000	0.0755	0.0000	1.0500
2	1	5	63.3289	29.4225	2.1326	0.0000	0.5000	0.0000	3.0000

2	1	7	31.8742	14.6779	8.0000	0.0000	0.1000	0.0000	1.5559	
2	1	9	84.0006	45.0000	0.6271	0.0000	3.0000	0.0000	1.0000	
2	2	2	0.0000	27.9213	5.8635	0.0000	0.0000	0.0000	1.0400	
2	2	3	0.0000	15.0000	2.2970	0.0000	0.0000	0.0000	1.3268	
2	2	4	0.0000	0.0019	6.0000	0.0000	0.0000	0.0000	1.0400	
2	2	7	0.0000	34.3910	1.7927	0.0000	-0.3560	0.0000	1.7376	
2	2	9	0.0000	26.3327	4.6867	0.0000	0.8177	0.0000	1.0404	
2	3	2	77.3619	4.8342	7.1628	0.0000	2.9933	0.0000	1.5948	
2	3	3	75.6935	25.0000	2.0000	0.0000	1.0000	0.0000	1.1680	
2	3	4	75.6201	18.7919	0.9833	0.0000	0.1218	0.0000	1.0500	
2	3	5	90.0000	17.5000	3.5000	0.0000	1.9770	0.0000	3.0000	
2	3	7	83.3202	43.6629	6.3865	0.0000	2.9392	0.0000	1.1266	
2	3	9	29.3808	16.2484	2.5832	0.5000	0.0100	0.0000	1.9017	
2	4	2	70.8687	12.0168	5.0132	0.0000	0.0222	0.0000	1.1243	
2	4	3	81.3686	40.0712	2.2396	0.0000	0.0222	0.0000	1.0369	
2	4	4	83.0104	43.4766	1.5328	0.0000	0.0222	0.0000	1.0500	
2	5	2	83.8555	5.1317	0.4377	0.0000	0.5000	0.0000	3.0000	
2	5	5	97.0064	32.1121	2.0242	0.0000	0.5000	0.0000	2.8568	
2	7	2	115.2319	50.0000	1.6748	0.0000	0.6983	0.0000	1.1000	
2	7	3	32.0466	49.7995	4.1312	0.5000	1.4682	0.0000	1.1000	
2	7	7	180.0000	-25.0000	20.0057	0.0000	1.4000	0.0000	1.1000	
2	9	2	106.3969	30.0000	0.9614	0.0000	1.9664	0.0000	2.2693	
2	9	9	180.0000	-27.2489	8.3752	0.0000	0.8112	0.0000	1.0004	
3	1	3	77.7473	40.1718	2.9802	-25.3063	1.6170	-46.1315	2.2503	
3	1	4	73.9544	12.4661	7.0000	0.0000	3.0000	0.0000	1.1880	
3	1	6	70.0000	35.0000	2.0000	0.0000	1.0000	0.0000	1.2500	
3	1	7	105.7527	28.9984	9.4291	0.0000	-0.4379	0.0000	1.1000	
3	1	9	70.0000	25.0000	1.0000	0.0000	1.0000	0.0000	1.2500	
3	2	3	0.0000	4.4124	2.5758	0.0000	0.0000	0.0000	2.9884	
3	2	4	0.0000	0.0019	6.0000	0.0000	0.0000	0.0000	1.0400	
3	2	7	0.0000	48.3620	2.0000	0.0000	1.0000	0.0000	1.2500	
3	2	9	0.0000	7.1233	1.9895	0.5000	0.3233	0.0000	1.1000	
3	3	3	80.7324	30.4554	0.9953	0.0000	1.6310	50.0000	1.0783	
3	3	4	84.3637	31.4554	0.9953	0.0000	1.6310	0.0000	1.0783	
3	3	5	83.9753	31.0715	3.5590	0.0000	0.8161	0.0000	1.1776	
3	3	7	88.7743	46.3505	1.2281	0.0000	0.6601	0.0000	1.7101	
3	3	9	90.0000	31.1442	5.0000	0.0000	0.5686	0.0000	2.0931	
3	4	3	74.1978	42.1786	1.7845	-18.0069	1.6777	0.0000	1.0500	
3	4	4	74.8600	43.7354	1.1572	-0.9193	1.6777	0.0000	1.0500	
3	5	3	81.0957	22.5308	7.4511	-2.3089	2.8609	0.0000	2.0914	
3	7	3	54.6586	42.2173	0.5000	0.0000	0.3706	0.0000	1.3157	
3	7	7	94.9741	41.1348	2.2450	0.0000	0.1218	0.0000	1.9235	
3	9	3	49.6374	27.4219	1.6709	0.0000	0.0369	0.0000	2.5673	

0	1	1	0	39.2561	2.4303	3.7193	0.0000	0.8924	0.0000	1.9950
0	1	2	0	106.3969	30.0000	0.9614	0.0000	1.9664	0.0000	2.2693
0	1	4	0	0.0000	26.3327	4.6867	0.0000	0.8177	0.0000	1.0404
0	1	5	0	0.0000	60.0000	1.8471	0.0000	0.6331	0.0000	1.8931
0	1	6	0	30.3748	1.0000	4.8528	0.0000	0.1019	0.0000	3.1660
0	2	2	0	180.0000	-27.2489	8.3752	0.0000	0.8112	0.0000	1.0004
0	2	3	0	97.5742	10.9373	2.5200	0.0000	1.8558	0.0000	1.0000
0	2	4	0	0.0000	0.2811	1.1741	0.0000	0.9136	0.0000	3.8138
0	2	5	0	84.0006	45.0000	0.6271	0.0000	3.0000	0.0000	1.0000
0	3	3	0	29.3808	16.2484	2.5832	0.5000	0.0100	0.0000	1.9017
0	3	4	0	70.0000	25.0000	1.0000	0.0000	1.0000	0.0000	1.2500
0	3	5	0	70.0000	25.0000	1.0000	0.0000	1.0000	0.0000	1.2500
0	4	4	0	70.0000	25.0000	1.0000	0.0000	1.0000	0.0000	1.2500
0	5	5	0	0.0000	7.1233	1.9895	0.5000	0.3233	0.0000	1.1000
0	6	6	0	-0.5000	53.0886	-0.1335	-6.2875	-1.9524	0.0000	0.0000
1	1	1	1	-0.4614	29.0459	0.2551	-4.8555	-2.7007	0.0000	0.0000
1	1	1	2	-0.2833	31.2867	0.2965	-4.8828	-2.4652	0.0000	0.0000
1	1	1	3	-0.3495	22.2142	-0.2959	-2.5000	-1.9066	0.0000	0.0000
1	1	1	6	0.0646	24.3195	0.6259	-3.9603	-1.0000	0.0000	0.0000
1	1	1	7	-0.5456	5.5756	0.8433	-5.1924	-1.0180	0.0000	0.0000
1	1	1	9	1.7555	27.9267	0.0072	-2.6533	-1.0000	0.0000	0.0000
1	1	3	1	-1.4358	36.7830	-1.0000	-8.1821	-1.0000	0.0000	0.0000
1	1	3	2	-1.3959	34.5053	0.7200	-2.5714	-2.1641	0.0000	0.0000
1	1	3	3	-2.5000	70.0597	1.0000	-3.5539	-2.9929	0.0000	0.0000
1	1	9	1	0.6852	11.2819	-0.4784	-2.5000	-2.1085	0.0000	0.0000
1	1	9	2	0.1933	80.0000	1.0000	-4.0590	-3.0000	0.0000	0.0000
1	3	3	1	-1.9889	76.4820	-0.1796	-3.8301	-3.0000	0.0000	0.0000
1	3	3	2	0.2160	72.7707	-0.7087	-4.2100	-3.0000	0.0000	0.0000
1	3	3	3	-2.5000	71.0772	0.2542	-3.1631	-3.0000	0.0000	0.0000
2	1	1	2	2.5000	-0.6002	1.0000	-3.4297	-2.8858	0.0000	0.0000
2	1	1	3	-2.5000	-3.3822	0.7004	-5.4467	-2.9586	0.0000	0.0000
2	1	1	6	2.5000	-4.0000	0.9000	-2.5000	-1.0000	0.0000	0.0000
2	1	1	7	1.2329	-4.0000	1.0000	-2.5000	-1.7479	0.0000	0.0000
2	1	1	9	0.8302	-4.0000	-0.7763	-2.5000	-1.0000	0.0000	0.0000
2	1	3	1	-2.5000	-4.0000	1.0000	-2.5000	-1.0000	0.0000	0.0000
2	1	3	2	0.0000	0.0000	0.0000	0.0000	0.0000	0.0000	0.0000
2	1	3	3	0.0000	0.0000	0.0000	0.0000	0.0000	0.0000	0.0000
2	1	9	1	0.0000	0.1000	0.0200	-2.5415	0.0000	0.0000	0.0000
2	3	1	7	0.0000	50.0000	0.3000	-4.0000	-2.0000	0.0000	0.0000
2	3	3	2	0.5511	25.4150	1.1330	-5.1903	-1.0000	0.0000	0.0000
2	3	3	3	-2.4242	128.1636	0.3739	-6.6098	-2.0000	0.0000	0.0000
2	3	3	7	0.0000	0.1000	0.0200	-2.5415	0.0000	0.0000	0.0000
2	3	5	3	1.4816	55.6641	0.0004	-7.0465	-2.7203	0.0000	0.0000
2	3	7	7	-0.3244	27.7086	0.0039	-2.8272	-2.0000	0.0000	0.0000

3	1	1	3	-5.5181	8.9706	0.0004	-6.1782	-2.0000	0.0000	0.0000
3	1	3	1	3.3423	30.3435	0.0365	-2.7171	0.0000	0.0000	0.0000
3	1	3	2	-0.0555	-5.0000	0.1515	-2.2056	0.0000	0.0000	0.0000
3	1	3	3	0.0000	0.0000	0.0000	0.0000	0.0000	0.0000	0.0000
3	3	3	3	0.5000	0.1000	0.4683	-11.5274	-1.7255	0.0000	0.0000
4	1	4	4	0.0000	49.3871	0.2000	-10.5765	-1.7255	0.0000	0.0000
6	1	1	6	-0.5000	95.4727	-0.2080	-4.8579	-1.7255	0.0000	0.0000
7	1	1	7	4.0000	45.8264	0.9000	-4.0000	0.0000	0.0000	0.0000
7	3	3	7	4.0000	45.8264	0.9000	-4.0000	0.0000	0.0000	0.0000
9	1	1	9	0.0000	0.0100	0.0100	-5.2275	0.0000	0.0000	0.0000
9	3	3	9	2.5000	8.9261	2.0000	-2.5710	-1.0000	0.0000	0.0000
9		! Nr	of hydrogen bonds;at1;at2;at3;Rhb;Dehb;vhb1							
3	2	3	2.1845	-2.3549	3.0582	19.1627				
3	2	4	1.6658	-3.8907	3.0582	19.1627				
3	2	5	1.5000	-2.0000	3.0582	19.1627				
4	2	3	1.8738	-3.5421	3.0582	19.1627				
4	2	4	1.8075	-4.1846	3.0582	19.1627				
4	2	5	1.5000	-2.0000	3.0582	19.1627				
5	2	3	1.5000	-2.0000	3.0582	19.1627				
5	2	4	1.5000	-2.0000	3.0582	19.1627				
5	2	5	1.5000	-2.0000	3.0582	19.1627				

Table S2. The peak positions and coordination number of O and Ni around the first shell of Ni from integrating the first peak of Fig. S15 and Fig. S16.

	Peak Position (Å)			Coordination Number (N)		
	NiO	Lithiation	Delithiation	NiO	Lithiation	Delithiation
Ni-Ni	3.075	2.675	2.975	10.19	7.13	7.37
Ni-O	1.875	1.925	1.875	3.23	1.20	2.59
O-Li					1.82	

SI Reference

1. Mueller JE, van Duin ACT, Goddard III WA (2010) Competing, coverage-dependent decomposition pathways for C_2H_y species on nickel (111). *J. Phys. Chem. C* 114: 20028-20041.
2. Han SS, van Duin ACT, Goddard III WA, Lee HM (2005) Optimization and application of lithium parameters for the reactive force field, ReaxFF. *J. Phys. Chem. A* 109: 4575-4582.
3. Hummers WS, Offeman RE (1958) Preparation of graphitic oxide. *J. Am. Chem. Soc.* 80: 1339-1339.
4. Park S, *et al.* (2008) Graphene oxide papers modified by divalent ions-enhancing mechanical properties via chemical cross-linking. *ACS Nano* 2: 572-578.
5. Park S, *et al.* (2009) Colloidal suspensions of highly reduced graphene oxide in a wide variety of organic solvents. *Nano Lett.* 9: 1593-1597.
6. Stankovich S, Piner RD, Nguyen ST, Ruoff RS (2006) Synthesis and exfoliation of isocyanate-treated graphene oxide nanoplatelets. *Carbon* 44: 3342-3347.
7. Murugan AV, Muraliganth T, Manthiram A (2009) Rapid, facile microwave-solvothermal synthesis of graphene nanosheets and their polyaniline nanocomposites for energy storage. *Chem. Mater.* 21: 5004-5006.